The metabolic co-regulator PGC1α suppresses prostate cancer metastasis

Veronica Torrano[1,18], Lorea Valcarcel-Jimenez[1,18], Ana Rosa Cortazar[1], Xiaojing Liu[2], Jelena Urosevic[3], Mireia Castillo-Martin[4,5], Sonia Fernández-Ruiz[1], Giampaolo Morciano[6], Alfredo Caro-Maldonado[1], Marc Guiu[3], Patricia Zúñiga-García[1], Mariona Graupera[7], Anna Bellmunt[3], Pahini Pandya[8], Mar Lorente[9], Natalia Martín-Martín[1], James David Sutherland[1], Pilar Sanchez-Mosquera[1], Laura Bozal-Basterra[1], Amaia Zabala-Letona[1], Amaia Arruabarrena-Aristorena[1], Antonio Berenguer[10], Nieves Embade[1], Aitziber Ugalde-Olano[11], Isabel Lacasa-Viscasillas[12], Ana Loizaga-Iriarte[12], Miguel Unda-Urzaiz[12], Nikolaus Schultz[13], Ana Maria Aransay[1,14], Victoria Sanz-Moreno[8], Rosa Barrio[1], Guillermo Velasco[9], Paolo Pinton[6], Carlos Cordon-Cardo[4], Jason W. Locasale[2,19], Roger R. Gomis[3,15,19] and Arkaitz Carracedo[1,16,17,20]

Cellular transformation and cancer progression is accompanied by changes in the metabolic landscape. Master co-regulators of metabolism orchestrate the modulation of multiple metabolic pathways through transcriptional programs, and hence constitute a probabilistically parsimonious mechanism for general metabolic rewiring. Here we show that the transcriptional co-activator peroxisome proliferator-activated receptor gamma co-activator 1α (PGC1α) suppresses prostate cancer progression and metastasis. A metabolic co-regulator data mining analysis unveiled that PGC1α is downregulated in prostate cancer and associated with disease progression. Using genetically engineered mouse models and xenografts, we demonstrated that PGC1α opposes prostate cancer progression and metastasis. Mechanistically, the use of integrative metabolomics and transcriptomics revealed that PGC1α activates an oestrogen-related receptor alpha (ERRα)-dependent transcriptional program to elicit a catabolic state and metastasis suppression. Importantly, a signature based on the PGC1α–ERRα pathway exhibited prognostic potential in prostate cancer, thus uncovering the relevance of monitoring and manipulating this pathway for prostate cancer stratification and treatment.

The metabolic switch in cancer encompasses a plethora of discrete enzymatic activities that must be coordinately altered to ensure the generation of biomass, reductive power and the remodelling of the microenvironment[1–4]. Despite the existence of mutations in metabolic enzymes[5], it is widely accepted that the main trigger for metabolic reprogramming is the alteration in cancer genes that remodel the signalling landscape[2]. Numerous reports provide evidence of the pathways regulating one or a few enzymes within a metabolic pathway in cancer. However, the means of coordinated regulation of complex metabolic networks remain poorly documented.

Master transcriptional co-regulators of metabolism control a variety of genes that are in charge of remodelling the metabolic landscape, and their impact in cellular and systemic physiology has been studied for decades. It is worth noting that these co-regulators,

[1]CIC bioGUNE, Bizkaia Technology Park, Building 801A, 48160 Derio, Bizkaia, Spain. [2]Department of Pharmacology and Cancer Biology, Duke Cancer Institute, Duke Molecular Physiology Institute, Duke University School of Medicine, Durham, North Carolina 27710, USA. [3]Oncology Programme, Institute for Research in Biomedicine (IRB Barcelona), The Barcelona Institute of Science and Technology, Barcelona 08028, Catalonia, Spain. [4]Department of Pathology, Icahn School of Medicine at Mount Sinai, New York, New York 10029, USA. [5]Department of Pathology, Fundação Champalimaud, 1400-038 Lisboa, Portugal. [6]Department of Morphology, Surgery and Experimental Medicine, Section of Pathology, Oncology and Experimental Biology, University of Ferrara, 44100, Italy. [7]Vascular Signalling Laboratory, Institut d'Investigació Biomèdica de Bellvitge (IDIBELL), Gran Via de l'Hospitalet 199-203, 08907 L'Hospitalet de Llobregat, Barcelona, Spain. [8]Tumour Plasticity Team, Randall Division of Cell and Molecular Biophysics, King's College London, New Hunt's House, Guy's Campus, London SE1 1UL, UK. [9]Department of Biochemistry and Molecular Biology I, School of Biology, Complutense University and Instituto de Investigaciones Sanitarias San Carlos (IdISSC), 28040 Madrid, Spain. [10]Biostatistics/Bioinformatics Uni, IRB Barcelona, Parc Científic de Barcelona, 08028 Barcelona, Spain. [11]Department of Pathology, Basurto University Hospital, 48013 Bilbao, Spain. [12]Department of Urology, Basurto University Hospital, 48013 Bilbao, Spain. [13]Computational Biology, Memorial Sloan-Kettering Cancer Center, New York 10065, USA. [14]Centro de Investigación Biomédica en Red de Enfermedades Hepáticas y Digestivas (CIBERehd). [15]Institució Catalana de Recerca i Estudis Avançats (ICREA), 08010 Barcelona, Spain. [16]Ikerbasque, Basque Foundation for Science, 48011 Bilbao, Spain. [17]Biochemistry and Molecular Biology Department, University of the Basque Country (UPV/EHU), PO Box 644, E-48080 Bilbao, Spain. [18]These authors contributed equally to this work. [19]These authors jointly supervised this work.
[20]Correspondence should be addressed to A.C. (e-mail: acarracedo@cicbiogune.es)
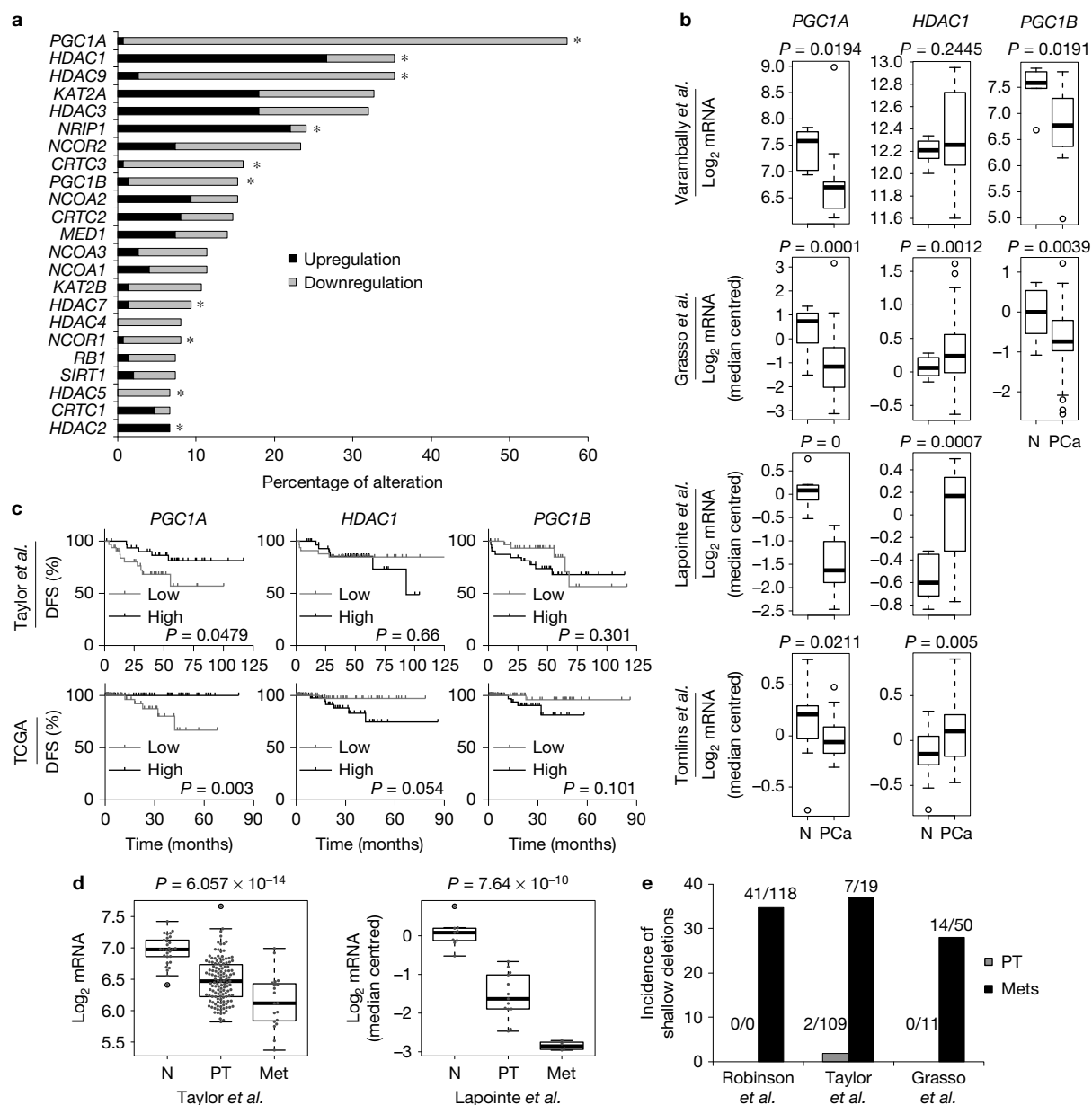
Figure 1 *PGC1A* is downregulated in prostate cancer. (**a**) Frequency of alterations (differences greater than twofold versus mean expression of non-tumoral biopsies) in the expression of 23 master co-regulators of metabolism in a cohort of 150 PCa patients[22]. *$P < 0.05$, statistically different expression of the indicated gene in PCa ($n = 150$) versus normal ($n = 29$) patient specimens (according to Supplementary Fig. 1A). (**b**) Gene expression levels of *PGC1A*, *PGC1B* and *HDAC1* in up to four additional PCa data sets (N, normal; PCa, prostate cancer). Sample sizes: Tomlins *et al.*[23] (N, 23; PCa, 52); Grasso *et al.*[21] (N, 12; PCa, 76); Lapointe *et al.*[18] (N, 9; PCa, 17); and Varambally *et al.*[24] (N, 6; PCa, 13). (**c**) Association of the indicated genes with disease-free survival (DFS) in two PCa data sets (low: first quartile distribution; high: fourth quartile distribution. Sample sizes: TCGA provisional data[19,20], primary tumours $n = 240$; Taylor *et al.*[22], primary tumours $n = 131$. (**d**) *PGC1A* expression in normal prostate (N), primary tumour (PT) and metastatic (Met) specimens in the Taylor and Lapointe data sets[18,22]. Sample sizes: Taylor (N, 29; PT, 131; Met, 19) and Lapointe (N, 9; PT, 13; Met, 4). (**e**) Incidence of *PGC1A* shallow deletions in three independent data sets (Robinson *et al.*[25], Taylor *et al.* and Grasso *et al.*). Points outlined by circles indicate statistical outliers (**d**). Error bars represent minimum and maximum values (**b,d**). *P*, *P* value. Statistical tests: two-tailed Student's *t*-test (**a,b**), Kaplan–Meier estimator (**c**) and ANOVA (**d**).

through their capacity to interact and regulate diverse transcription factors, exhibit a unique capacity to control complex and extensive transcriptional networks, making them ideal candidates to promote or oppose oncogenic metabolic programs.

The tumour suppressor PTEN is a negative regulator of cell growth, transformation and metabolism[6–9]. PTEN and its main downstream

pathway, PI(3)K, have been extensively implicated in prostate cancer (PCa) pathogenesis and progression[10–12]. This tumour suppressor is progressively lost through the progression of PCa, and complete loss of PTEN is predominant in advanced disease and metastasis[8]. Genetically engineered mouse models (GEMMs) recapitulate many of the features of PCa progression. However, the molecular and
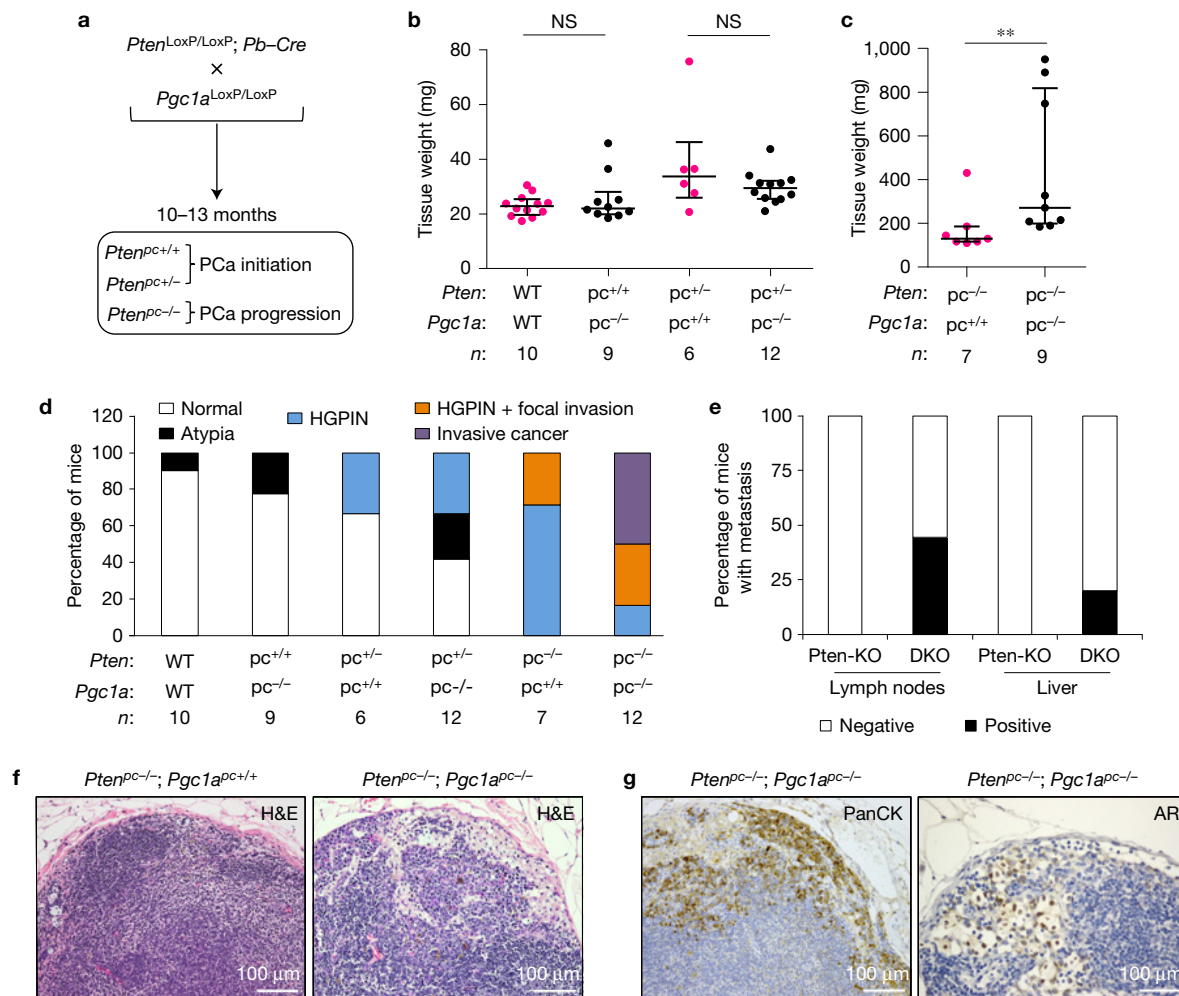
Figure 2 Combined deletion of *Pgc1a* and *Pten* in the murine prostate epithelia results in prostate cancer progression and dissemination. (**a**) Schematic representation of the genetic cross and the time of analysis. (**b**,**c**) Comparison of anterior prostate lobe weights (when both anterior lobes were analysed, the average weight was calculated and represented) between genotypes. *n* = number of mice; pc, prostate-specific allelic changes; +, wild-type allele; −, deleted allele; WT, any given genotype resulting in the lack of deletion of *Pgc1a* or *Pten* alleles. (**d**) Histopathological characterization of the prostate (HGPIN, high-grade prostatic intraepithelial neoplasia) in the indicated genotypes. (**e**) Quantification of the frequency of metastatic lesions in lymph nodes and liver of *Pten*-KO (5) and DKO (9) mice. (**f**) Representative histological images (×200 magnification) of lymph nodes with (right) and without (left) metastasis in the indicated genotypes. (**g**) Representative immunohistochemical detection (×200 magnification) of Pan-cytokeratin (panCK)- and androgen receptor (AR)-positive cells in metastatic lymph nodes of DKO mice. *Pten*-KO, *Pten^pc−/−^ Pgc1a^pc+/+^*; DKO, *Pten^pc−/−^ Pgc1a^pc−/−^*. NS, not significant; **P < 0.01. H&E, haematoxylin–eosin. Error bars indicate interquartile range (**b**,**c**). Statistical test: two-tailed Mann–Whitney *U*-test (**b**,**c**).

metabolic bases for PCa metastasis remain poorly understood[13–16]. Indeed, complete loss of PTEN in the mouse prostate does not result in metastasis[11], in turn suggesting that additional critical events are required in this process.

In this study, we designed a bioinformatics analysis to interrogate multiple PCa data sets encompassing hundreds of well-annotated specimens. This approach allowed us to define a master regulator of PCa metabolism that is crucial for the progression of the disease. Our results identify the peroxisome proliferator-activated receptor gamma co-activator 1 alpha (PGC1α) as a suppressor of PCa metastasis. This transcriptional co-activator exerts its function through the regulation of oestrogen-related receptor alpha (ERRα) activity, in concordance with the activation of a catabolic program and the inhibition of PCa metastasis.

RESULTS

A bioinformatics screen identifies *PGC1A* as a metabolic co-regulator associated with prostate cancer progression

We approached the study of PCa metabolism applying criteria to ensure the selection of relevant master regulators that contribute to the metabolic switch. We focused on transcriptional co-regulators of metabolism[17] that were consistently altered in several publicly available PCa data sets[18–24], and were associated with reduced time to recurrence and disease aggressiveness. We first evaluated the expression levels of the metabolic co-regulators in a study comprising 150 PCa specimens and 29 non-pathological prostate tissues (or controls)[22]. The analysis revealed 10 co-regulators in the set of study with significant differential expression in PCa compared with non-neoplastic prostate tissue (Fig. 1a and Supplementary Fig. 1A).

We next extended this observation to four additional data sets[18,21,23,24] in which there were available data for non-tumoral and PCa tissues. Only the alteration in *PPARGC1A* (*PGC1A*), *PPARGC1B* (*PGC1B*) and *HDAC1* expression was further confirmed in most or all sets (Fig. 1b and Supplementary Fig. 1B). Among these, *PGC1A* was the sole co-regulator with altered expression associated with Gleason score (Supplementary Fig. 1C,D) and disease-free survival (Fig. 1c).

To rule out the possibility that cellular proliferation could contribute to the alteration of metabolic regulators, we carried out an additional analysis in which we compared the expression of *PGC1A* in PCa versus a benign hyper-proliferative condition (benign prostate hyperplasia or BPH). The results corroborated that the decrease in *PGC1A* expression is associated with a cancerous state rather than with a proliferative condition (Supplementary Fig. 1E).

We observed that the expression of *PGC1A* was progressively decreased from primary tumours to metastasis (Fig. 1d and Supplementary Fig. 1F). Strikingly, genomic analysis revealed shallow deletions of *PGC1A* exquisitely restricted to metastatic PCa specimens[19–22,25] (Fig. 1e), in full agreement with the notion that there is a selective pressure to reduce the expression of this transcriptional co-activator as the disease progresses.

From our analysis, PGC1α emerges as the main master metabolic co-regulator altered in PCa, with an expression pattern reminiscent of a tumour suppressor.

Pgc1a deletion in the murine prostate epithelium promotes prostate cancer metastasis

PGC1α has been widely studied in the context of systemic metabolism[26], whereas its activity in cancer is just beginning to be understood[27–33]. To ascertain the role of PGC1α in PCa *in vivo*, we conditionally deleted this metabolic co-regulator in the prostate epithelium[34], alone or in combination with loss of the tumour suppressor *Pten*[11] (Fig. 2a–d and Supplementary Fig. 2A,B). *Pgc1a* deletion alone or in the context of *Pten* heterozygosity did not result in any differential tissue mass or histological alteration, which led us to conclude that it is not an initiating event (Fig. 2b,d). However, compound loss of both *Pten* and *Pgc1a* resulted in significantly larger prostate mass (Fig. 2c), together with a remarkable increase in the rate of invasive cancer (Fig. 2d). Histological analysis of the prostate revealed the existence of vascular invasion in double-mutant mice (DKO), but not in *Pten*-deleted (*Pten*-KO) prostates (Supplementary Fig. 2C). PGC1α regulates the inflammatory response, which could influence and contribute to the phenotype observed[35]. However, we did not observe significant differences in the infiltration of polymorphonuclear neutrophils and lympho-plasmacytic infiltrates in our experimental settings (Supplementary Fig. 2D). PGC1α has been also shown to induce angiogenesis in coherence with the induction of vascular endothelial growth factor (VEGF)-A expression[36]. *Pgc1a* status in our GEMMs did not alter VEGF-A expression and microvessel density (Supplementary Fig. 2E,F). We therefore excluded the possibility that regulation of angiogenesis or inflammation downstream of PGC1α could drive the phenotype characterized in this study.

PCa GEMMs faithfully recapitulate many of the features of the human disease[37]. A reduced number of mouse models with clinically relevant mutations show increased metastatic potential[13–16]. Strikingly,

histopathological analysis of our mouse model in the context of *Pten* loss revealed that DKO mice—but not *Pten*-KO counterparts—presented evidence of metastasis, which was estimated in 44% to lymph nodes and 20% to liver (Fig. 2e,f and Supplementary Fig. 2G). Metastatic dissemination was in agreement with the observation of pan-cytokeratin (panCK)- and androgen receptor (AR)-positive PCa cell deposits in the lymph nodes of DKO mice (Fig. 2g). Of note, 33% of *Pten*-KO mice presented small groups of panCK-positive cells in lymph nodes (without metastatic lesions; Supplementary Fig. 2H), suggesting that even if these cells are able to reach the lymph nodes, they lack capacity to establish clinical metastasis. Interestingly, bone analysis revealed disseminated groups (but not clinical metastasis) of panCK-positive cells in DKO but not in *Pten*-KO mice (Supplementary Fig. 2I–K). Analysis of a small cohort of *Pten*[pc−/−]; *Pgc1a*[pc+/−] mice demonstrated that heterozygous loss of *Pgc1a* is sufficient to promote aggressiveness, vascular invasion and metastasis (Supplementary Fig. 2L–N). This observation supports the notion that single-copy loss of *PGC1A* (as observed in metastatic human PCa specimens, Fig. 1e) could be a key contributing factor to the metastatic phenotype.

The cooperative effect observed in our mouse model between loss of *Pten* and *Pgc1a* was supported by the direct correlation of the two transcripts in patient specimens and the association of *PGC1A* downregulation with *PTEN* genomic loss (TCGA provisional data[19,20], Supplementary Fig. 2O).

In summary, our results in GEMMs and patient data sets formally demonstrate that the downregulation of PGC1α in PCa is an unprecedented causal event for the progression of the disease and its metastatic dissemination.

PGC1α suppresses prostate cancer growth and metastasis

To characterize the prostate tumour suppressive activity of PGC1α, we first evaluated its expression level in well-established PCa cell lines[38]. Using previously reported PGC1α-positive and -negative melanoma cells[28], we could demonstrate that PCa cell lines lack detectable expression of the transcriptional co-activator at the protein level (Fig. 3a). In agreement with this notion, PGC1α silencing in these cells failed to impact on the expression of its well-established targets[39] (Supplementary Fig. 3A). Importantly, through the analysis of publicly available data sets[22], we could demonstrate that the transcript levels of *PGC1A* in metastatic cell lines are comparable to those observed in human metastatic PCa specimens and vastly reduced compared with PGC1α-positive melanoma cells (Fig. 3a and Supplementary Fig. 3B). Despite our efforts to optimize the detection of the protein with different commercial antibodies, we could not identify an immunoreactive band that would correspond to PGC1α, in contrast with other reports[40,41]. Yet, we cannot rule out that in non-basal conditions, stimulation of other factors such as AR[41] or 5′ AMP-activated protein kinase (AMPK)[40] could lead to the upregulation and allow detection of PGC1α in PCa cells.

Owing to the lack of PGC1α detection in PCa cellular systems, we aimed at reconstituting the expression of this gene to levels achievable in the cancer cell lines previously reported[28]. By means of lentiviral delivery of inducible Pgc1α and doxycycline titration, we reached expression levels of this protein in three PCa cell lines (AR-dependent—LnCaP—and independent—PC3 and DU145)
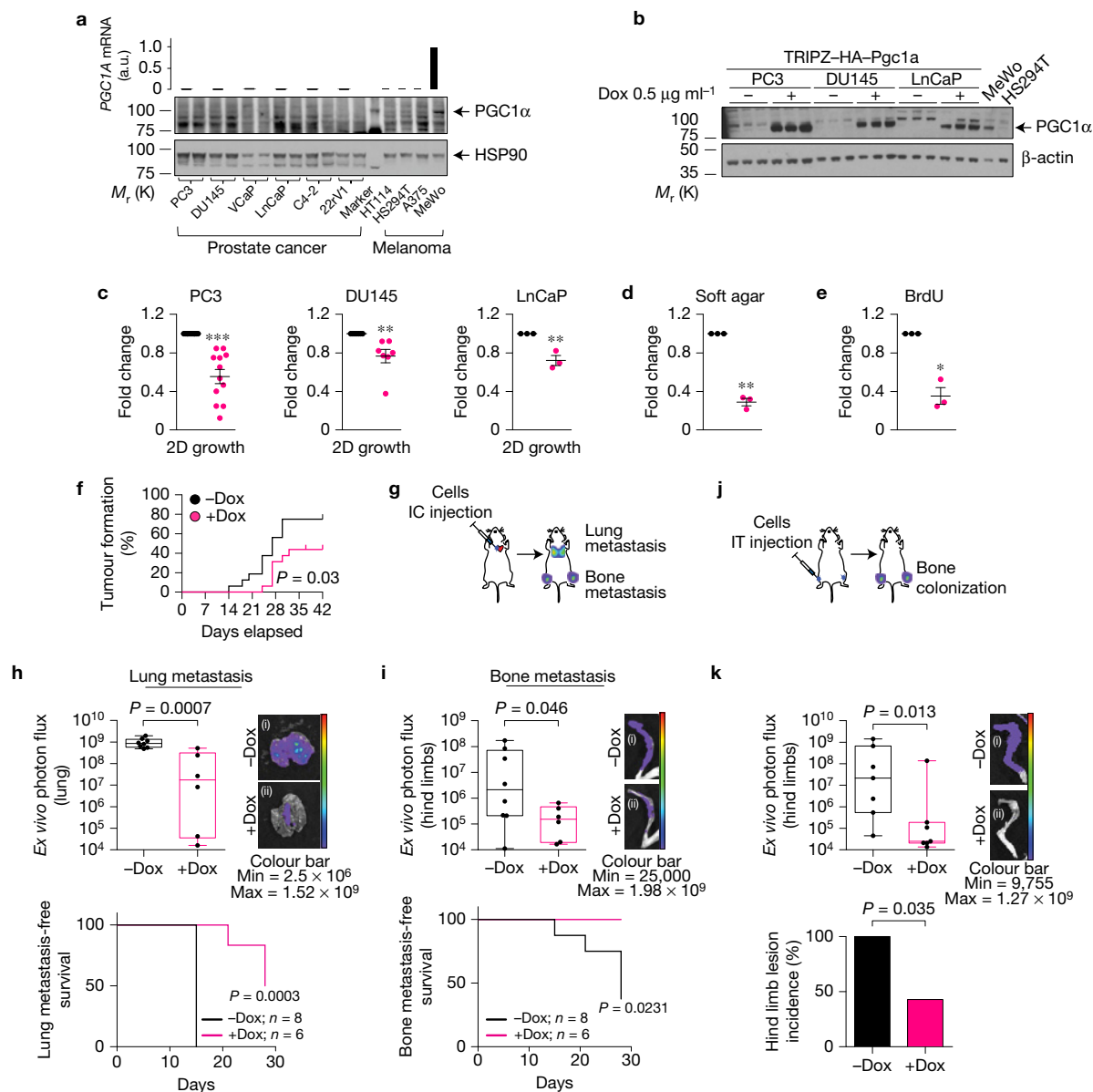
Figure 3 PGC1α exhibits tumour and metastasis suppressive activity in PCa cell lines. (**a**) Analysis of PGC1α expression by quantitative rtPCR (top histogram) and western blot in a panel of prostate cancer cell lines (technical duplicates are shown), using melanoma cell lines as positive (MeWo) and negative (HT114, HS294T and A375) controls ($n = 3$, independent experiments). (**b**) Representative experiment of PGC1α expression in PC3, DU145 and LnCaP cell lines after treatment with $0.5 \, \mu g \, ml^{-1}$ doxycycline (Dox) (similar results were obtained in three independent experiments). (**c**) Relative cell number quantification in Pgc1α-expressing (+Dox, pink) and -non-expressing (−DOX, black) cells. Data are represented as cell number at day 6 relative to −Dox cells ($n = 12$ in PC3; $n = 7$ in DU145; $n = 3$ in LnCaP, independent experiments). (**d,e**) Effect of Pgc1α expression on anchorage-independent growth (**d**; $n = 3$, independent experiments) and BrdU incorporation (**e**; $n = 3$, independent experiments) in PC3 cells. (**f**) Evaluation of tumour formation capacity in xenotransplantation experiments ($n = 7$ mice; two injections per mouse). (**g**) Schematic representation of metastasis assay through intra-cardiac (IC) injection. (**h,i**) Evaluation of metastatic capacity of Pgc1α-expressing PC3 cells using IC xenotransplant assays ($n = 8$ mice for −Dox and $n = 6$ for +Dox). Luciferase-dependent signal intensity (upper panels) and metastasis-free survival curves (lower panels) of PCa cells in lungs (**h**) and limbs (**i**) were monitored for up to 28 days. Representative luciferase images are presented, referring to the quantification plots. In hind limb photon flux analysis, the average signal from two limbs per mouse is presented. Images (i) and (ii) depict tibia or lung photon flux images from specimens that are proximal to the median signal in −Dox and +Dox, respectively. (**j**) Schematic representation of bone metastasis assay through intra-tibial (IT) injection. (**k**) Evaluation of the metastatic capacity of Pgc1α-expressing PC3 cells using IT xenotransplant assays ($n = 7$ mice). Photon flux quantification at 20 days (upper panel) and incidence of metastatic lesions at the end point (lower panel). Representative luciferase images are presented, referring to the quantification plots. For photon flux analysis, the average signal from two limbs per mouse is presented. For incidence analysis, mice with at least one limb yielding luciferase signal >50,000 units were considered metastasis-positive. Images (i) and (ii) depict tibia photon flux images from specimens that are proximal to the median signal in −Dox and +Dox, respectively. +Dox, Pgc1α-induced conditions; −Dox, Pgc1α-non-expressing conditions; BrdU, bromo deoxyuridine; a.u., arbitrary units. Error bars represent s.e.m. (**c–e**) or minimum and maximum values (**h,i,k**). Statistical tests: two-tailed Student's *t*-test (**c–e**), one-tailed Mann–Whitney *U*-test (**h,i,k** (upper panels)), log-rank test (**f,h,i** (lower panels)) and Fisher's exact test (**k**, lower panels). *$P < 0.05$, **$P < 0.01$, ***$P < 0.001$. Statistics source data for Fig. 3k are provided in Supplementary Table 9. Unprocessed original scans of blots are shown in Supplementary Fig. 8.
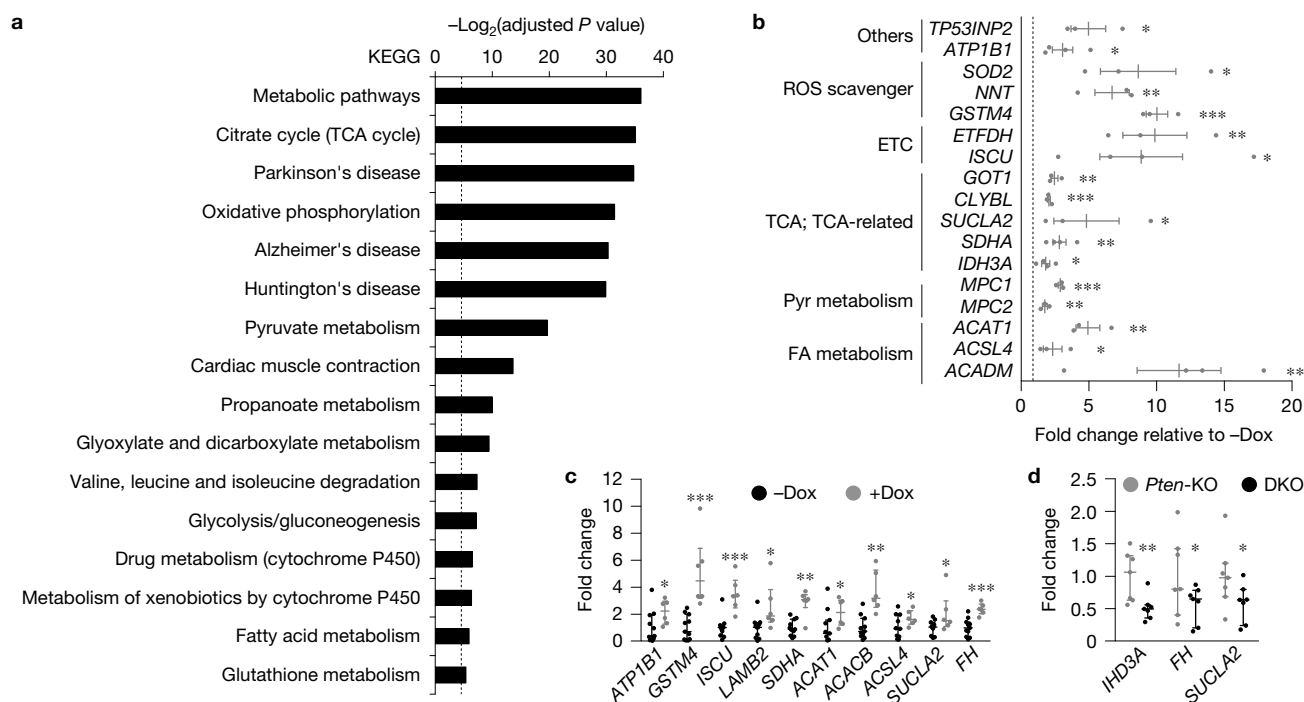
Figure 4 PGC1α induces a metabolic transcriptional program. (**a**) KEGG (Kyoto Encyclopaedia of Genes and Genomes) analysis of the transcriptional program regulated by PGC1α. The dotted line indicates $P = 0.05$. (**b–d**) Validation of microarray by quantitative rtPCR in PC3 TRIPZ–HA–Pgc1α cells (**b**, $n = 3$ for *TP53INP2*, *SOD2*, *NNT*, *GSTM4*, *ETFDH*, *GOT1*, *CLYBL*, *SUCLA2*, *MPC1*, *MPC2*, *ACAT1* and *ACSL4*; $n = 4$ for *ATP1B1*, *ISCU*, *SDHA*, *IDH3A* and *ACADM*; independent experiments; data are normalized to the −Dox condition, represented by a black dotted line), xenograft samples (**c**, −Dox $n = 11$ tumours; +Dox $n = 6$ tumours) and prostate tissue samples from *Pten*-KO and DKO mice (**d**, $n = 7$ mice). +Dox, Pgc1α-induced conditions; −Dox, Pgc1α-non-expressing conditions; *Pten*-KO, *Pten$^{pc−/−}$*-*Pgc1a$^{pc+/+}$*; DKO, *Pten$^{pc−/−}$*, *Pgc1a$^{pc−/−}$*. ROS, reactive oxygen species; ETC, electron transport chain; TCA, tricarboxylic acid cycle; Pyr, pyruvate; FA, fatty acid. Error bars indicate s.e.m. (**b**) or interquartile range (**c**,**d**). Statistical tests: one-tail Student's *t*-test (**b**); one-tail Mann–Whitney *U*-test (**c**,**d**). *$P < 0.05$, **$P < 0.01$, ***$P < 0.001$.

equivalent to that observed in the PGC1α-expressing melanoma cell line MeWo (Fig. 3b and Supplementary Fig. 3C,D). Next, we evaluated the cellular outcome of expressing PGC1α in PCa cell lines. Interestingly, expression of Pgc1α in this context resulted in a reduction in bi-dimensional and three-dimensional growth (Fig. 3c,d and Supplementary Fig. 3E), cellular proliferation (Fig. 3e and Supplementary Fig. 3F) and cell cycle progression (Supplementary Fig. 3G). Of note, we excluded the possibility that doxycycline treatment could influence the result of the growth analysis (Supplementary Fig. 3H). The Pgc1α phenotype was recapitulated *in vivo*, where ectopic expression of this gene decreased tumour formation and growth (Fig. 3f and Supplementary Fig. 3I–K). In agreement with the GEMM data, we did not observe a contribution of angiogenesis to the phenotype (Supplementary Fig. 3L–N).

We observed in GEMMs that *Pgc1a* loss resulted in metastatic dissemination (Fig. 2). We next sought to study whether Pgc1α expression could oppose a pre-existing metastatic phenotype. To this end, we carried out xenotransplant assays in immunocompromised mice using luciferase-expressing Pgc1α-inducible PC3 cells. Intra-cardiac injection of these cells (Fig. 3g) revealed that Pgc1α expression blunted metastatic growth in the lung, and led to a remarkable decrease in bone colonization (Fig. 3h,i). As an additional approach, we sought to analyse metastatic tumour re-initiation capacity by means of local injection of PCa cells at the metastatic site. As PCa exhibits an osteotropic nature[42], we carried out intra-tibial injection

of cells and the appearance of tumour masses in the bone was monitored[43] (Fig. 3j). The results demonstrated that PGC1α exerts a potent anti-metastatic activity both in bone tumour mass and metastatic lesions (Fig. 3k). These data provide evidence of the anti-metastatic potential of PGC1α.

PGC1α determines the oncogenic metabolic wiring in prostate cancer

PGC1α regulates gene expression through the interaction with diverse transcription factors[26]. To define the transcriptional program associated with the tumour suppressive activity of PGC1α, we performed gene expression profiling from Pgc1α-expressing versus -non-expressing PC3 cells. We identified 174 probes with significantly altered signal encoding genes predominantly related to functions such as mitochondrial catabolic programs and energy-producing processes[26,44] (Supplementary Table 1 and Fig. 4a), which we validated by quantitative real-time PCR (rtPCR) (Fig. 4b–d and Supplementary Fig. 4).

To demonstrate that the tumour suppressive activity of PGC1α was indeed accompanied by a global metabolic rewiring, we carried out integrative metabolomics. We analysed cell line, xenograft and GEMM tissue extracts using liquid-chromatography high-resolution mass spectrometry (LC–HRMS). LC–HRMS metabolomics and subsequent biochemical assays confirmed that oxidative processes such as fatty acid β-oxidation (Fig. 5a–d and Supplementary Fig. 5A–C and
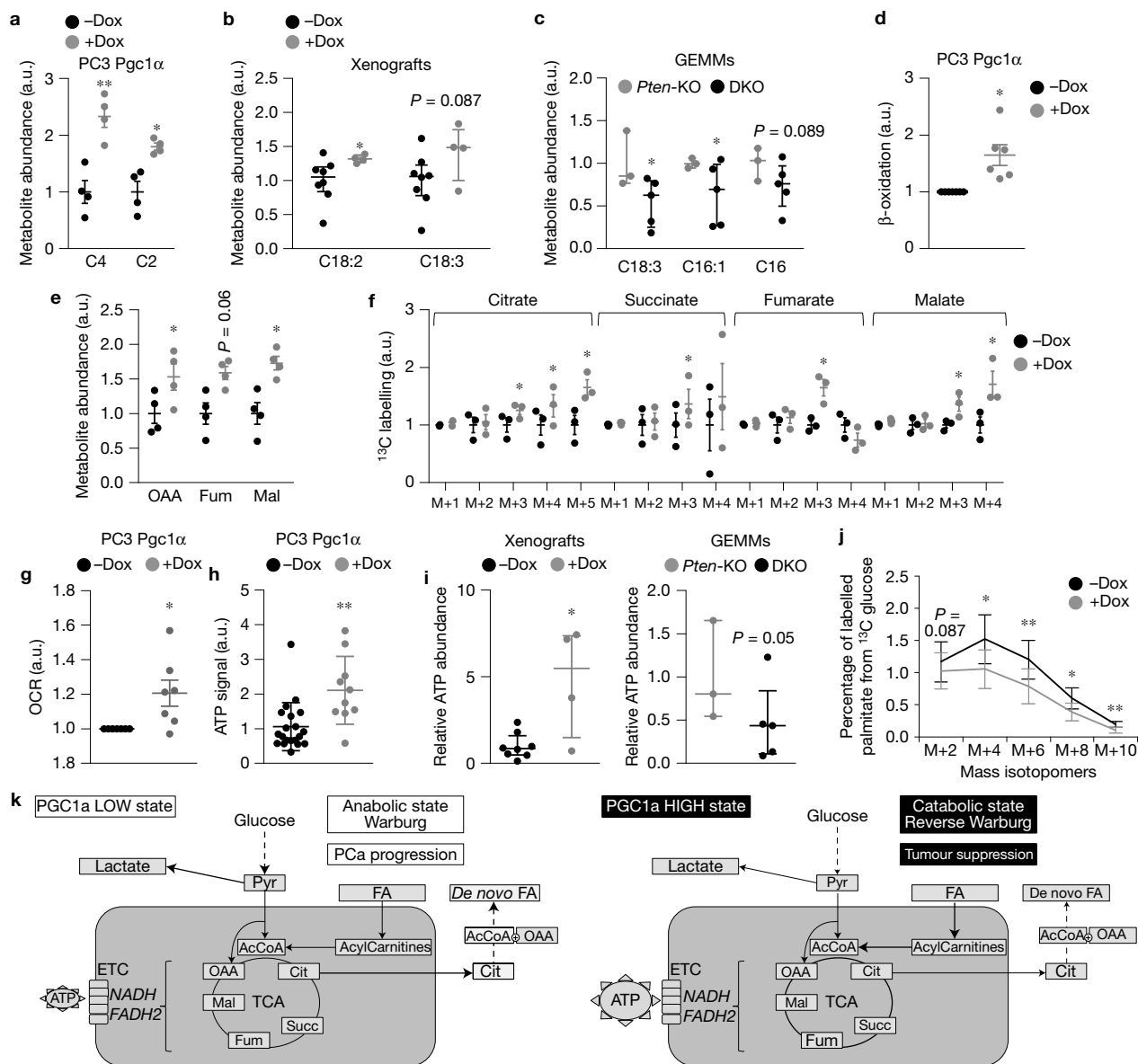
Figure 5 PGC1α induces a catabolic metabolic program. (**a–c**) Untargeted LC–HRMS analysis of differential abundance in metabolites involved in fatty acid catabolism in Pgc1α-expressing PC3 cells (**a**, $n=4$, independent experiments), xenografts (**b**, −Dox $n=8$ tumours; +Dox $n=4$ tumours) and GEMMs (**c**, Pten KO $n=3$ mice; DKO $n=5$ mice). (**d**) Evaluation of the dehydrogenation of tritiated palmitate (readout of fatty acid β-oxidation) in Pgc1α-expressing PC3 cells ($n=6$, independent experiments). (**e**) Effect of Pgc1α expression on the abundance of tricarboxylic acid cycle (TCA) intermediates measured by LC–HRMS in PC3 cells ($n=4$, independent experiments). (**f**) Effect of Pgc1α expression on TCA intermediates (mass isotopomer abundance) after stable ^{13}C–U$_6$-glucose labelling in PC3 cells ($n=3$, independent experiments). (**g**) Oxygen consumption rate (OCR) in PC3 Pgc1α-expressing cells ($n=7$, independent experiments). (**h**) Basal

mitochondrial ATP production in PC3 cells following Pgc1α expression ($n=20$ for −Dox and $n=10$ for +Dox conditions, independent experiments). (**i**) LC–HRMS quantification of ATP abundance in xenografts (left panel, −Dox $n=8$ tumours; +Dox $n=4$ tumours) and GEMMs (right panel, Pten-KO $n=3$ mice; DKO $n=5$ mice). (**j**) Effect of Pgc1α expression on palmitate paired mass isotopomer abundance after stable ^{13}C–U$_6$-glucose labelling in PC3 cells ($n=3$, independent experiments). (**k**) Schematic representation of the main findings of the study. Pyr, pyruvate; AcCoA, acetyl CoA; OAA, oxaloacetate; Mal, malate; Fum, fumarate; Succ, succinate; Cit, citrate; ETC, electron transport chain; FA, fatty acids. a.u., arbitrary unit. Error bars indicate s.e.m. (**a,d–h,j**) or interquartile range (**b,c,i**). Statistical tests: two-tailed Student's t-test (**a,d–h,j**); one-tail Mann–Whitney U-test (**b,c,i**). $^*P<0.05,^{**}P<0.01,^{***}P<0.001$.

Supplementary Tables 2–5) and tricarboxylic acid cycle (TCA, Fig. 5e and Supplementary Fig. 5D) were increased in response to Pgc1α expression. To quantitatively define the use of glucose in the TCA cycle, we carried out stable ^{13}C–U$_6$-glucose isotope labelling. This experimental approach provided definitive evidence of the increased oxidation of glucose in the mitochondria in Pgc1α-expressing cells

(Fig. 5f). This metabolic wiring was consistent with elevated oxygen consumption (basal and ATP-producing) and ATP levels following Pgc1α expression (Fig. 5g–i and Supplementary Fig. 5E–I and Supplementary Tables 2–5).

We next reasoned that over-activation of mitochondrial oxidative processes would lead to decreased anabolic routes. On the one hand,

we monitored the incorporation of carbons from $^{13}C-U_6$-glucose into fatty acids (through the export of citrate from TCA to the cytoplasm[45] and conversion to acetyl CoA that is used for *de novo* lipid synthesis). Interestingly, we found a significant decrease in ^{13}C incorporation into palmitate (reflected as ^{13}C carbon pairs) when Pgc1α was expressed (Fig. 5j and Supplementary Fig. 5J). On the other hand, we monitored lactate production as a readout of aerobic glycolysis or 'the Warburg effect'[2], which has been associated with the anabolic switch. As predicted, Pgc1α-expressing cells exhibited reduced extracellular lactate levels (Supplementary Fig. 5K). Of note, lactate production and respiration were unaltered by doxycycline challenge in non-transduced PC3 cells (Supplementary Fig. 5L,M). Taken together, our data provide a metabolic basis for the tumour suppressive potential of PGC1α in PCa, according to which this metabolic co-regulator controls the balance between catabolic and anabolic processes (Fig. 5k).

An ERRα-dependent transcriptional program mediates the prostate tumour suppressive activity of PGC1α

We next aimed to identify the transcription factor that mediated the activity of PGC1α, and hence we performed a promoter enrichment analysis. The results revealed a predominant abundance in genes regulated by ERRα (Fig. 6a). We corroborated these results with Gene Set Enrichment Analysis (GSEA; normalized enrichment score = 2.02; nominal P value = 0.0109)[46]. This transcription factor controls a wide array of metabolic functions, from oxidative processes to mitochondrial biogenesis[44]. We have shown that PGC1α is indeed capable of regulating functions attributed to ERRα, such as mitochondrial oxidative metabolism (Figs 4 and 5 and Supplementary Figs 4 and 5). In addition, we observed that Pgc1a expression led to increased mitochondrial volume (Supplementary Fig. 6A). To ascertain the extent to which the growth inhibitory and anti-metastatic activity of PGC1α required its ability to interact with ERRα, we took advantage of a mutant variant of the co-activator (PGC1α^L2L3M) that is unable to interact with this and other nuclear receptors[46,47]. The expression of PGC1α^L2L3M in PC3 cells (Supplementary Fig. 6B) failed to upregulate target genes, to reprogram oxidative metabolism, to inhibit cell growth, and, importantly, to suppress bone metastasis in intra-tibial xenografts (Fig. 6b–f and Supplementary Fig. 6C). To further discriminate between PGC1α functions that depend on ERRα or other nuclear receptors, we undertook a targeted silencing approach, and we transduced Pgc1α-inducible PC3 cells with an ERRα-targeting or a scramble short hairpin RNA (shRNA; Supplementary Fig. 6D). In coherence with the L2L3M mutant data, ERRα silencing partially blunted the effects of Pgc1α on gene expression and cell growth (Fig. 6g and Supplementary Fig. 6H). *In vivo*, silencing of ERRα in the presence of the ectopically expressed transcriptional co-activator resulted in a significant increase in bone metastasis incidence from 40% (in Pgc1α-expressing cells transduced with scramble shRNA) to full penetrance (Fig. 6h). Of note, the requirement of ERRα for the effect of PGC1α was recapitulated *in vitro* with a reverse agonist of the transcription factor, namely XCT790[48] (Supplementary Fig. 6F–I).

It is worth noting that other metabolic pathways have been suggested to sustain the metastatic phenotype. Oxidative stress has been shown to limit metastatic potential in breast cancer

and melanoma[29,49]. PGC1α regulates the expression of antioxidant genes, and the enhancement of mitochondrial metabolism can lead to the production of reactive oxygen species[28,29,49] (ROS; Fig. 4b and Supplementary Table 1). We therefore tested whether ROS production was modified in our experimental settings and if it could contribute to the phenotype observed. Mitochondrial and cellular ROS production were not consistently altered by Pgc1α expression *in vitro* (Supplementary Fig. 6J). In addition, lipid peroxidation (which serves as a readout of ROS production) was unaffected in our xenograft study (Supplementary Fig. 6K). These results are coherent with the inability of antioxidants to rescue the proliferative defect elicited by Pgc1α (Supplementary Fig. 6L).

Our data provide a molecular mechanism by which ERRα activation downstream of PGC1α promotes a metabolic rewiring that suppresses PCa proliferation and metastasis.

A PGC1α–ERRα transcriptional signature harbours prognostic potential

We have shown that reduced *PGC1A* expression in PCa exhibits prognostic potential (Fig. 1c). As our data demonstrate that transcriptional regulation downstream of ERRα is key for the tumour suppressive activity of this co-activator, we reasoned that the association of PGC1α with aggressiveness and disease-free survival should be recapitulated when monitoring ERRα target genes (Fig. 7a). We started the analysis from the list of genes positively regulated by PGC1α in our cellular system (153 genes, Fig. 7b). As predicted, the analysis in two independent patient data sets confirmed that the average signal of the PGC1α gene list was positively correlated with time to PCa recurrence (Fig. 7c). In addition, we observed a decrease in the expression of the aforementioned gene list associated with disease initiation and progression (Supplementary Fig. 7A). Importantly, comparable results were obtained when we performed the analysis with the subset of ERRα-target genes within the PGC1α gene set (73 genes, Supplementary Table 6 and Fig. 7b,d and Supplementary Fig. 7B). We next sought to curate the gene list to consolidate a prognostic PGC1α-ERRα gene set. We therefore focused on genes that exhibited a strong correlation with *PGC1A* in patient data sets. We selected genes that were significantly correlated with the co-activator ($R > 0.2$; $p < 0.05$) in at least three out of five studies. The results unveiled a PGC1α transcriptional signature in patients consisting of 17 genes, most of which exhibited decreased expression in PCa versus BPH, and were further downregulated in metastatic disease (Supplementary Table 7 and Supplementary Fig. 7C,D). Nearly 60% of these genes were regulated by ERRα (10 genes out of 17) and were selected for further analysis as a PGC1α–ERRα curated gene set (Supplementary Table 7). The results revealed reduced PGC1α–ERRα curated gene set expression as the disease progressed (Fig. 7e). We next analysed the association of the PGCα–ERRα curated gene set with disease recurrence. To this end, we compared patients harbouring primary tumours with ERRα curated gene set average signal values in the first quartile (Q1, termed signature-positive) versus the rest (Q2–Q4). Patients with signature-positive tumours exhibited reduced disease-free survival in two independent data sets (Fig. 7f). A hazard ratio of 4.2 (Taylor) and 17.8 (TCGA) was defined for signature-positive patients, whereas signature-negative individuals presented reduced risk of recurrence, with a hazard ratio
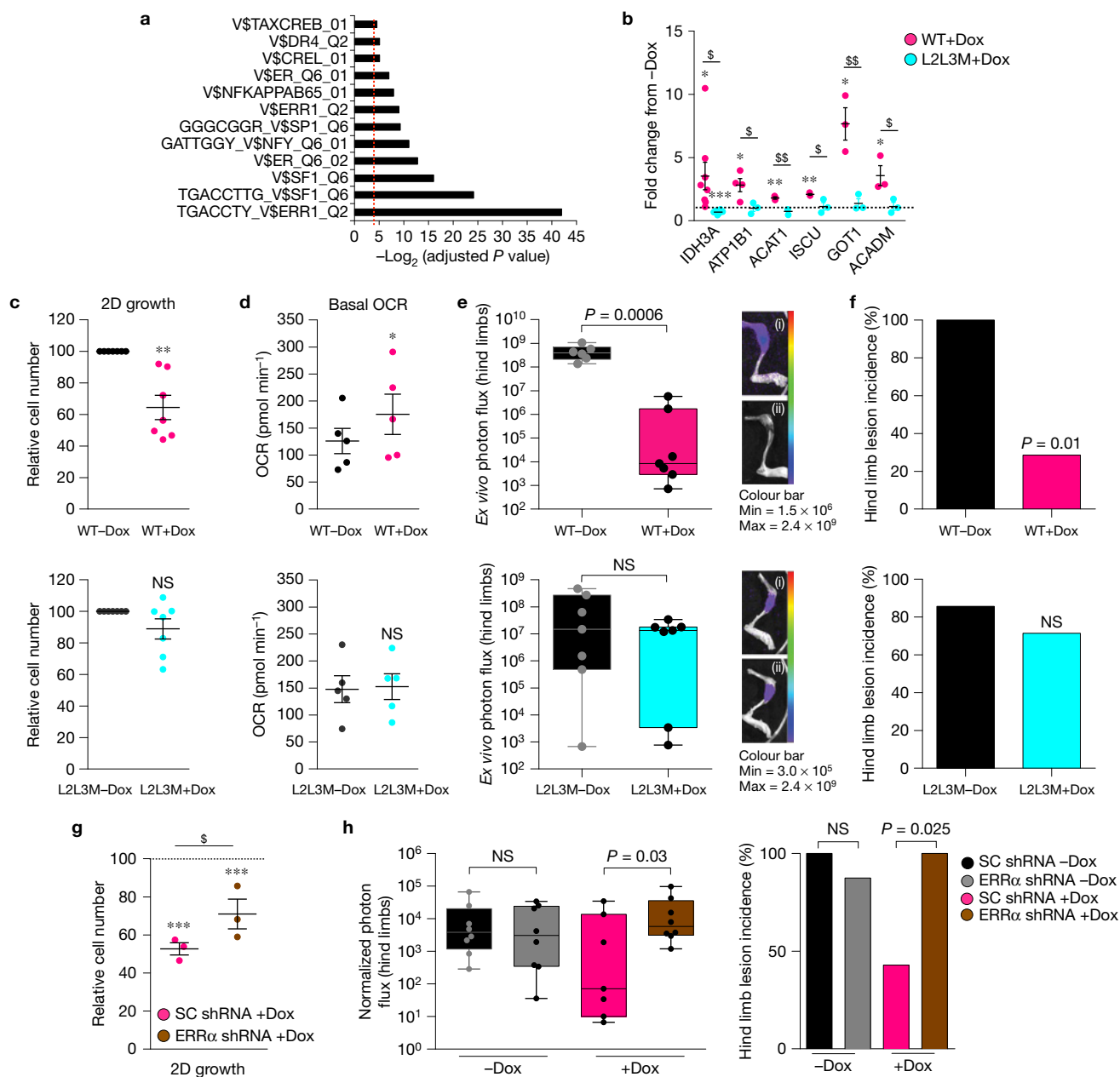
Figure 6 An ERRα-dependent transcriptional program mediates the tumour suppressive activity of PGC1α. (**a**) Promoter enrichment analysis of the PGC1α transcriptional program. The red dotted line indicates $P = 0.05$. (**b–d**) Effect of Pgc1α^{WT} (WT) or Pgc1α^{L2L3M} (L2L3M) induction on the expression of the indicated genes (**b**, quantitative rtPCR; $n = 8$ for IDH3A; $n = 4$ for *ATP1B1*; $n = 3$ for *ACAT1*, *ISCU*, *GOT1* and *ACADM* genes, independent experiments; data are normalized to each −Dox condition, represented by a black dotted line), relative cell number by crystal violet (**c**, $n = 7$, independent experiments) and oxygen consumption rate (**d**, OCR, $n = 5$, independent experiments). (**e,f**) Evaluation of the metastatic capacity of PC3 Pgc1α^{WT} (WT)-expressing (upper panels) or PC3 Pgc1α^{L2L3M} (L2L3M)-expressing (lower panels) cells using intra-tibial xenotransplant assays (**e**, photon flux quantification; WT, $n = 6$ mice; L2L3M, $n = 7$ mice, two hind limbs per mouse; **f**, incidence of metastatic lesions presented as histograms). Representative luciferase images are presented referring to the quantification plots. For photon flux analysis, average signal from two limbs per mouse is presented. For incidence analysis, mice with at least one limb yielding luciferase signal >50,000 units were considered metastasis-positive. Images (i) and (ii) depict tibia photon flux images from specimens

that are proximal to the median signal in −Dox and +Dox, respectively. (**g**) Relative cell number quantification following ERRα silencing in Pgc1α-expressing PC3 cells. Data are represented as cell number at day 4 relative to −Dox cells ($n = 3$, independent experiments). (**h**) Evaluation of metastatic capacity of Pgc1α-expressing PC3 cells transduced with SC shRNA or ERRα shRNA using intra-tibial implantation for 14 days ($n = 8$ mice; two injections per mouse; incidence of metastatic lesions presented as histograms). For photon flux analysis (left panel), average signal from two limbs per mouse is presented. For incidence analysis (right panel), mice with at least one limb yielding luciferase signal >50,000 units were considered metastasis-positive. +Dox, Pgc1α-induced conditions; −Dox, Pgc1α-non-expressing conditions. NS, not significant; SC, Scramble; OCR, oxygen consumption rate. Error bars represent s.e.m. (**b–d,g**) or minimum and maximum values (**e,h**). Statistical tests: one-tailed Student's *t*-test (**b–d,g**); one-tailed Mann–Whitney *U*-test (**e,h** (left panel)); Fisher's exact test (**f,h** (right panel)). * or $^{\$}P < 0.05$, ** or $^{\$\$}P < 0.01$, ***$P < 0.001$. Asterisks indicate statistical difference between −Dox and +Dox conditions and dollar symbols between Pgc1α^{WT} and Pgc1α^{L2L3M} or SC shRNA and ERRα shRNA. Statistics source data for Fig. 6e,h are provided in Supplementary Table 9.
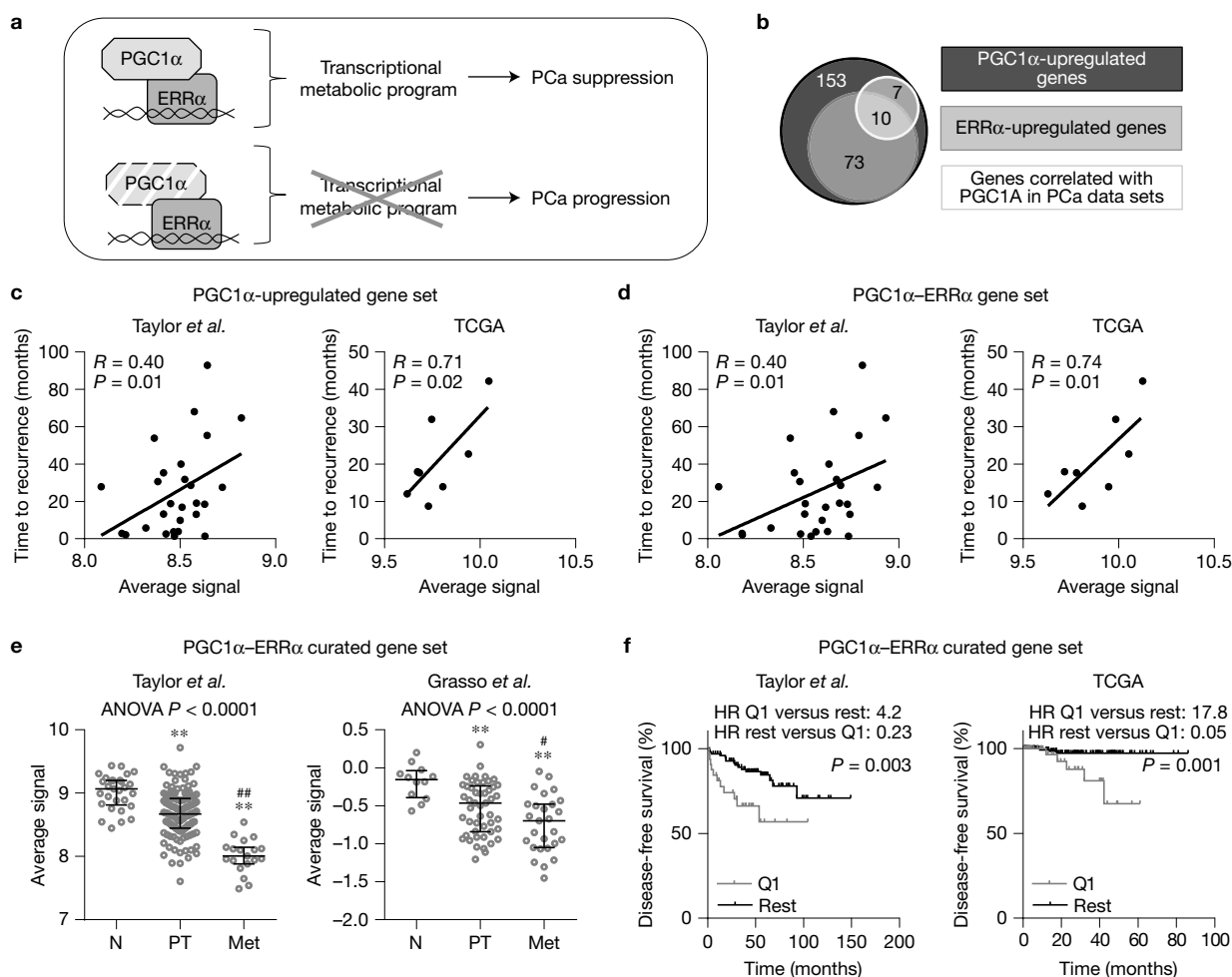
Figure 7 The PGC1α transcriptional program is associated with prostate cancer recurrence. (**a**) Schematic summary of the ERRα-dependent regulation of the PGC1α transcriptional metabolic program and its association with PCa progression. Dashed PGC1α outline represents a decrease in abundance. (**b**) Venn diagram showing the distribution of PGC1α target genes, ERRα target genes (from Supplementary Table 6) and genes correlated with *PGC1A* expression in PCa patient specimens (from Supplementary Table 7). (**c,d**) Correlation between time to recurrence and the average signal of the genes within the PGC1α-upregulated gene set (**c**) or the PGC1α-dependent ERRα-upregulated gene set (**d**) in the indicated data sets (Taylor[22] n = 27; TCGA provisional data set[19,20] n = 8). Each dot corresponds to an individual patient specimen. (**e**) Representation of the average signal of the genes within

the PGC1α–ERRα curated gene set (Supplementary Table 7) in normal tissue (N; Taylor n = 29 and Grasso[21] n = 12), primary tumour (PT; Taylor n = 131 and Grasso n = 49) and metastasis specimens (Met; Taylor n = 19 and Grasso n = 27), in two independent data sets. Each dot corresponds to an individual patient specimen. (**f**) Association of the PGC1α–ERRα signature with disease-free survival in the indicated patient data sets (Taylor n = 131; TCGA provisional data set n = 240). Q1 indicates patients with signature signal within the first quartile of primary tumours (Q1) in the corresponding data set. HR, hazard ratio. Error bars indicate interquartile range. Statistical tests: Pearson's coefficient (R) (**c,d**), ANOVA (**e**), Student's t-test (**e**) and Kaplan–Meier estimator (**f**). **P < 0.01; #P > 0.05. Asterisk indicates statistical difference versus N; hash indicates statistical difference versus PT.

of 0.23 (Taylor) and 0.05 (TCGA). Furthermore, the frequency of patients with signature-positive signal values was absent or low in the normal prostate group and further increased in metastasis compared with primary tumours (Supplementary Fig. 7E). Taken together, ERRα-regulated metabolic transcriptional program is associated with the activity of PGC1α in PCa. This interplay is conserved in patient specimens and defines a gene signature that harbours prognostic potential.

DISCUSSION

In this study we provide a comprehensive analysis of master transcriptional co-regulators of metabolism in PCa. Through the use of human data mining analysis, GEMMs and cellular systems, our

study presents evidence demonstrating that PGC1α exerts a tumour suppressive activity opposing PCa metastasis. Interestingly, three out of ten significantly altered co-regulators (*PGC1A*, *PGC1B* and *NRIP1*, Fig. 1a) in the Taylor[22] PCa data set (two out of three consistently altered throughout databases, Fig. 1b) converge in the regulation of a common transcriptional metabolic program, led by ERRα (ref. 44), and that is associated with the phenotype observed in this study. These data strongly suggest that such pathway is of critical importance for the control of aggressiveness properties in PCa. Indeed, our results demonstrate that a gene set composed of ERRα target genes that are under the control of PGC1α expression is progressively downregulated in PCa and metastatic disease, and presents prognostic potential for the identification of patients at risk of early recurrence.

The study of the tumour suppressive potential of Pgc1α in mouse models allowed us to characterize a clinically relevant PCa GEMM presenting enhanced metastatic dissemination. PGC1α is added to the shortlist of genetic events that drive metastasis in this model[13–16], and the first to be explicitly linked to the regulation of the metabolic switch. Overall, our finding is of importance for the future study of the requirements for PCa metastasis and therefore for therapeutic purposes.

The sole alteration of PGC1α expression in PCa has a profound impact on the oncogenic metabolic switch[50]. These data are in line with the reported activities of this protein in metabolism and mitochondrial biogenesis[26]. Of note, despite the widely accepted fact that the reported metabolic switch[50] has comparable consequences in all cancer scenarios, the study of PGC1α in other tumour types has also revealed a selective pressure towards oxidative processes[27–29]. Previous work from others and us defined PGC1α signalling as a selective advantage for breast cancer and melanoma cells[4,27–29,51]. The contribution of this co-activator to cellular proliferation differs between tumour types and experimental systems, promoting growth in melanoma[28] but irrelevant to breast cancer cells[29]. Interestingly, in breast circulating tumour cells, PGC1α expression supports metastatic capacity[29]. The molecular pathways regulating these diverse biological features converge in the activation of ERRα and peroxisome proliferator-activated receptors (PPAR). Whereas PPAR activation mediates the increase in fatty acid β-oxidation[4], ERRα is responsible for the overall increase in oxidative metabolism and mitochondrial biogenesis[44]. Similarly, the activation of an antioxidant transcriptional program has been suggested to contribute to anoikis and cancer cell dissemination in a PGC1α-dependent and independent manner[27,28,49,52]. In PCa, however, we demonstrate that the oxidative metabolic program elicited by PGC1α prevents tumour growth and metastatic dissemination, in the absence of overt changes in ROS production, inflammatory response or angiogenic signals. These findings support the notion that the optimal metabolic wiring for tumour growth and metastasis might differ depending on the tumour type, the mutational landscape of the tumour and, potentially, the microenvironment. This would lead to opposite activities of PGC1α depending on the cancer setting, from metastatic promoter[29] to metastasis suppressor (as we demonstrate in the present work).

In summary, our study identifies PGC1α as a master regulator of PCa metabolism that opposes the dissemination of the disease. Therefore, a PGC1α-regulated ERRα-dependent transcriptional program might open new avenues in the identification of metabolic transcriptional signatures that can be exploited for patient stratification and the use of metabolism-modulatory therapies. □

METHODS
Methods and any associated references are available in the online version of the paper.

Note: Supplementary Information is available in the online version of the paper

AUTHOR CONTRIBUTIONS
V.T. and L.V.-J. performed all *in vitro* and *in vivo* experiments, unless specified otherwise. A.R.C. carried out the bioinformatic and biostatistical analysis. A.Berenguer and N.S. provided support and advice in data set retrieval and normalization. S.F.-R. performed the histochemical stainings. P.S.-M. and S.F.-R. performed genotyping analyses. X.L. and J.W.L. contributed to the experimental design and executed the metabolomic analyses. G.M. and P.Pinton performed the biochemical ATP measurement *in vitro* and mitochondria analysis. G.V., P.Z.-G. and M.L. performed or coordinated (G.V.) subcutaneous xenograft experiments. J.U., A.Bellmunt, M.Guiu and R.R.G. performed or coordinated (R.R.G.) the intra-cardiac and intra-tibial metastasis assays. R.R.G. contributed to the design of the patient gene signature analysis. M.Graupera carried out microvessel staining and quantifications. P.Pandya and V.S.-M. provided technical advice and contributed to *in vitro* analysis. N.M.-M., A.A.-A. and A.Z.-L. contributed to the experimental design and discussion. A.C.-M. and N.E. performed Seahorse assays. J.D.S. and R.B. performed or coordinated (R.B.) the cloning of *Pgc1a* in lentiviral vectors. C.C.-C. and M.C.-M. carried out the pathological analysis and scoring of the xenografts and GEMMs. A.U.-O., I.L.-V., A.L.-I. and M.U.-U. provided BPH and PCa samples for gene expression analysis from Basurto University Hospital. A.M.A. contributed to the discussion of the results. A.C. directed the project, contributed to data analysis and wrote the manuscript.

COMPETING FINANCIAL INTERESTS
The authors declare no competing financial interests.

1. Loo, J. M. *et al.* Extracellular metabolic energetics can promote cancer progression. *Cell* **160**, 393–406 (2015).
2. Vander Heiden, M. G., Cantley, L. C. & Thompson, C. B. Understanding the Warburg effect: the metabolic requirements of cell proliferation. *Science* **324**, 1029–1033 (2009).
3. Vander Heiden, M. G. *et al.* Evidence for an alternative glycolytic pathway in rapidly proliferating cells. *Science* **329**, 1492–1499 (2010).
4. Carracedo, A., Cantley, L. C. & Pandolfi, P. P. Cancer metabolism: fatty acid oxidation in the limelight. *Nat. Rev. Cancer* **13**, 227–232 (2013).
5. Yang, M., Soga, T. & Pollard, P. J. Oncometabolites: linking altered metabolism with cancer. *J. Clin. Invest.* **123**, 3652–3658 (2013).
6. Ortega-Molina, A. *et al.* Pten positively regulates brown adipose function, energy expenditure, and longevity. *Cell Metab.* **15**, 382–394 (2012).
7. Garcia-Cao, I. *et al.* Systemic elevation of PTEN induces a tumor-suppressive metabolic state. *Cell* **149**, 49–62 (2012).
8. Salmena, L., Carracedo, A. & Pandolfi, P. P. Tenets of PTEN tumor suppression. *Cell* **133**, 403–414 (2008).
9. Song, M. S., Salmena, L. & Pandolfi, P. P. The functions and regulation of the PTEN tumour suppressor. *Nat. Rev. Mol. Cell Biol.* **13**, 283–296 (2012).
10. Di Cristofano, A., Pesce, B., Cordon-Cardo, C. & Pandolfi, P. P. Pten is essential for embryonic development and tumour suppression. *Nat. Genet.* **19**, 348–355 (1998).
11. Chen, Z. *et al.* Crucial role of p53-dependent cellular senescence in suppression of Pten-deficient tumorigenesis. *Nature* **436**, 725–730 (2005).
12. Majumder, P. K. *et al.* Prostate intraepithelial neoplasia induced by prostate restricted Akt activation: the MPAKT model. *Proc. Natl Acad. Sci. USA* **100**, 7841–7846 (2003).
13. Magnon, C. *et al.* Autonomic nerve development contributes to prostate cancer progression. *Science* **341**, 1236361 (2013).
14. Ding, Z. *et al.* SMAD4-dependent barrier constrains prostate cancer growth and metastatic progression. *Nature* **470**, 269–273 (2011).
15. Nandana, S. & Chung, L. W. Prostate cancer progression and metastasis: potential regulatory pathways for therapeutic targeting. *Am. J. Clin. Exp. Urol.* **2**, 92–101 (2014).
16. Cho, H. *et al.* RapidCaP, a novel GEM model for metastatic prostate cancer analysis and therapy, reveals myc as a driver of Pten-mutant metastasis. *Cancer Discov.* **4**, 318–333 (2014).
17. Mouchiroud, L., Eichner, L. J., Shaw, R. J. & Auwerx, J. Transcriptional coregulators: fine-tuning metabolism. *Cell Metab.* **20**, 26–40 (2014).
18. Lapointe, J. *et al.* Gene expression profiling identifies clinically relevant subtypes of prostate cancer. *Proc. Natl Acad. Sci. USA* **101**, 811–816 (2004).
19. Cerami, E. *et al.* The cBio cancer genomics portal: an open platform for exploring multidimensional cancer genomics data. *Cancer Discov.* **2**, 401–404 (2012).
20. Gao, J. *et al.* Integrative analysis of complex cancer genomics and clinical profiles using the cBioPortal. *Sci. Signal* **6**, pl1 (2013).
21. Grasso, C. S. *et al.* The mutational landscape of lethal castration-resistant prostate cancer. *Nature* **487**, 239–243 (2012).
22. Taylor, B. S. *et al.* Integrative genomic profiling of human prostate cancer. *Cancer Cell* **18**, 11–22 (2010).
23. Tomlins, S. A. *et al.* Integrative molecular concept modeling of prostate cancer progression. *Nat. Genet.* **39**, 41–51 (2007).
24. Varambally, S. *et al.* Integrative genomic and proteomic analysis of prostate cancer reveals signatures of metastatic progression. *Cancer Cell* **8**, 393–406 (2005).
25. Robinson, D. *et al.* Integrative clinical genomics of advanced prostate cancer. *Cell* **161**, 1215–1228 (2015).
26. Lin, J., Handschin, C. & Spiegelman, B. M. Metabolic control through the PGC-1 family of transcription coactivators. *Cell Metab.* **1**, 361–370 (2005).
27. Haq, R. *et al.* Oncogenic BRAF regulates oxidative metabolism via PGC1α and MITF. *Cancer Cell* **23**, 302–315 (2013).
28. Vazquez, F. *et al.* PGC1α expression defines a subset of human melanoma tumors with increased mitochondrial capacity and resistance to oxidative stress. *Cancer Cell* **23**, 287–301 (2013).
29. LeBleu, V. S. *et al.* PGC-1α mediates mitochondrial biogenesis and oxidative phosphorylation in cancer cells to promote metastasis. *Nat. Cell Biol.* **16**, 992–1003 (2014).
30. LaGory, E. L. *et al.* Suppression of PGC-1α is critical for reprogramming oxidative metabolism in renal cell carcinoma. *Cell Rep.* **12**, 116–127 (2015).
31. D'Errico, I. *et al.* Peroxisome proliferator-activated receptor-gamma coactivator 1-α (PGC1α) is a metabolic regulator of intestinal epithelial cell fate. *Proc. Natl Acad. Sci. USA* **108**, 6603–6608 (2011).
32. Sancho, P. *et al.* MYC/PGC-1α balance determines the metabolic phenotype and plasticity of pancreatic cancer stem cells. *Cell Metab.* **22**, 590–605 (2015).
33. Audet-Walsh, E. *et al.* The PGC-1α/ERRα axis represses one-carbon metabolism and promotes sensitivity to anti-folate therapy in breast cancer. *Cell Rep.* **14**, 920–931 (2016).
34. Lin, J. *et al.* Defects in adaptive energy metabolism with CNS-linked hyperactivity in PGC-1α null mice. *Cell* **119**, 121–135 (2004).
35. Eisele, P. S. & Handschin, C. Functional crosstalk of PGC-1 coactivators and inflammation in skeletal muscle pathophysiology. *Semin. Immunopathol.* **36**, 27–53 (2014).
36. Saint-Geniez, M. *et al.* PGC-1α regulates normal and pathological angiogenesis in the retina. *Am. J. Pathol.* **182**, 255–265 (2013).
37. Nardella, C., Carracedo, A., Salmena, L. & Pandolfi, P. P. Faithfull modeling of PTEN loss driven diseases in the mouse. *Curr. Top. Microbiol. Immunol.* **347**, 135–168 (2011).
38. Nardella, C. *et al.* Aberrant Rheb-mediated mTORC1 activation and Pten haploinsufficiency are cooperative oncogenic events. *Genes Dev.* **22**, 2172–2177 (2008).
39. Li, S. *et al.* Genome-wide coactivation analysis of PGC-1α identifies BAF60a as a regulator of hepatic lipid metabolism. *Cell Metab.* **8**, 105–117 (2008).
40. Tennakoon, J. B. *et al.* Androgens regulate prostate cancer cell growth via an AMPK-PGC-1α-mediated metabolic switch. *Oncogene* **33**, 5251–5261 (2014).
41. Shiota, M. *et al.* Peroxisome proliferator-activated receptor gamma coactivator-1α interacts with the androgen receptor (AR) and promotes prostate cancer cell growth by activating the AR. *Mol. Endocrinol.* **24**, 114–127 (2010).
42. Buijs, J. T. & van der Pluijm, G. Osteotropic cancers: from primary tumor to bone. *Cancer Lett.* **273**, 177–193 (2009).
43. Garcia, M. *et al.* Cyclooxygenase-2 inhibitor suppresses tumour progression of prostate cancer bone metastases in nude mice. *BJU Int.* **113**, E164–E177 (2014).
44. Feige, J. N. & Auwerx, J. Transcriptional coregulators in the control of energy homeostasis. *Trends Cell Biol.* **17**, 292–301 (2007).
45. Finley, L. W., Zhang, J., Ye, J., Ward, P. S. & Thompson, C. B. SnapShot: cancer metabolism pathways. *Cell Metab.* **17**, e462–466 (2013).
46. Stein, R. A. *et al.* Estrogen-related receptor alpha is critical for the growth of estrogen receptor-negative breast cancer. *Cancer Res.* **68**, 8805–8812 (2008).
47. Gaillard, S. *et al.* Receptor-selective coactivators as tools to define the biology of specific receptor-coactivator pairs. *Mol. Cell* **24**, 797–803 (2006).
48. Chang, C. Y. *et al.* The metabolic regulator ERRα, a downstream target of HER2/IGF-1R, as a therapeutic target in breast cancer. *Cancer Cell* **20**, 500–510 (2011).
49. Piskounova, E. *et al.* Oxidative stress inhibits distant metastasis by human melanoma cells. *Nature* **527**, 186–191 (2015).
50. Lunt, S. Y. & Vander Heiden, M. G. Aerobic glycolysis: meeting the metabolic requirements of cell proliferation. *Annu. Rev. Cell Dev. Biol.* **27**, 441–464 (2011).
51. Carracedo, A. *et al.* A metabolic prosurvival role for PML in breast cancer. *J. Clin. Invest.* **122**, 3088–3100 (2012).
52. Schafer, Z. T. *et al.* Antioxidant and oncogene rescue of metabolic defects caused by loss of matrix attachment. *Nature* **461**, 109–113 (2009).

METHODS

Reagents. 3-[4-(2,4-Bis-trifluoromethylbenzyloxy)-3-methoxyphenyl]-2-cyano-*N*-(5-trifluoromethyl-1,3,4-thiadiazol-2-yl)acrylamide (XCT 790), etomoxir (ETO), doxycycline hyclate (Dox), oligomycin, *N*-acetyl-cysteine (NAC) and manganese (III) tetrakis (4-benzoic acid)porphyrin chloride (MnTBAP) were purchased from Sigma.

Cell culture. Human prostate carcinoma cell lines LnCaP, DU145 and PC3 were purchased from Leibniz-Institut DSMZ - Deutsche Sammlung von Mikroorganismen und Zellkulturen GmbH, who provided an authentication certificate. None of the cell lines used in this study were found in the database of commonly misidentified cell lines maintained by ICLAC and NCBI Biosample. Cells were transduced with a modified TRIPZ (Dharmacon) doxycycline-inducible lentiviral construct in which the RFP and miR30 region was replaced by *HA–Flag–Pgc1a* (ref. 51) or *HA–Flag–Pgc1a*[1,2L,3M] (ref. 47). Lentiviral shRNA constructs targeting *PGC1A* (TRCN0000001166) and *ESRRA* (TRCN0000022180) were purchased from Sigma and a scramble shRNA (hairpin sequence: 5′-CCGGCA ACAAGATGAAGAGCACCAACTCGAGTTGGTGCTCTTCATCTTGTTG-3′) was used as the control. For *ESRRA* shRNAs, the puromycin resistance cassette was replaced by the hygromycin cassette from pLKO.1 Hygro (Addgene Ref. 24150) using BamHI and KpnI sites. Melanoma lines were provided by M. D. Boyano[53] and A. Buqué and purchased from ATCC. Cell lines were routinely monitored for mycoplasma contamination and quarantined while treated if positive.

Animals. All mouse experiments were carried out following the ethical guidelines established by the Biosafety and Welfare Committee at CIC bioGUNE and The Institutional Animal Care and Use Committee of IRB Barcelona. The procedures employed were carried out following the recommendations from AAALAC. Xenograft experiments were performed as previously described[54], injecting 10^6 cells per condition in two flanks per mouse. PC3 TRIPZ–HA-Pgc1a cells were injected in each flank of nude mice and 24 h post-injections mice were fed with chow or doxycycline diet (Research diets, D12100402). GEMM experiments were carried out as reported in a mixed background[11,14,55,56] (where the founder colony was cross-bred for at least three generations before the expansion of experimental cohorts to ensure a homogenous mixed background). The *Pten*[loxP] and *Pgc1a*[loxP] conditional knockout alleles have been described elsewhere[11,34]. Prostate epithelium-specific deletion was effected by the Pb–*Cre4*[11]. Mice were fasted for 6 h before tissue collection (9:00–15:00) to prevent metabolic alterations due to immediate food intake.

For intra-tibial and intra-cardiac injections BALB/c nude male mice (Harlan) of 9–11 weeks of age were used. Before the injections, PC3 Tripz–HA–Pgc1a (WT, L2L3M, SC shRNA, ERRα shRNA) cell lines were pre-treated for 48 h with PBS or doxycycline (0.5 µg ml⁻¹). Mice injected with cells treated with doxycycline were also pre-treated for 48 h with 1 mg ml⁻¹ of doxycycline in drinking water. After the injections this group of mice was left on continuous doxycycline treatment (1 mg ml⁻¹ in drinking water). Before the injections mice were anaesthetized with a mixture of ketamine (80 mg kg⁻¹) and xylazine (8 mg kg⁻¹). For intra-tibial injections, 1×10^4 cells were resuspended in a final volume of 5 µl of cold PBS and injected as described previously[57]. For intra-cardiac injections 2×10^5 cells were resuspended in a final volume of 100 µl of cold PBS and injected as described previously[57]. After the injections, tumour development was followed on a weekly basis by BLI using the IVIS-200 imaging system from Xenogen. Quantification of bioluminescent images was done with Living Image 2.60.1 software. The development of metastasis was confirmed by examining *in vivo* or *ex vivo* (following necropsy) bioluminescent images of organs of interest (metastasis positivity in lesion incidence analysis was defined as tibias with luciferase signals greater than 50,000 units). When comparing cell lines independently transduced with the luciferase-expressing vector (Fig. 6h), photon flux values per limb were presented as normalized signal (corrected by basal signal, obtained within 24 h after injection): Normalized photon flux = (day 14 signal/day 0 signal) × 1,000. For metastasis-free survival curves, a metastatic event was scored when the measured value of bioluminescence bypassed 1/10 of the day 0 value.

Patient samples. All samples were obtained from the Basque Biobank for research (BIOEF, Basurto University hospital) on informed consent and with evaluation and approval from the corresponding ethics committee (CEIC code OHEUN11-12 and OHEUN14-14).

Cellular, molecular and metabolic assays. Cell number quantification with crystal violet[58] was performed as referenced. Soft agar assays were performed as previously described (INSERT REF 60) seeding 5,000 cells per well in 6-well plates.

Western blot was performed as previously described[51]. Antibodies used: PGC1α (H300; Santa Cruz Biotechnology sc-13067; dilution 1:1,000); ERRα (E1G1J; Cell Signaling no. 13826; dilution 1:1,000); β-actin (clone AC-74; Sigma no. A 5316;

dilution 1:2,000); GAPDH (clone 14C10; Cell Signaling no. 2218; dilution 1:1,000); HSP90 (Cell Signaling; no. 4874; dilution 1:1,000).

RNA was extracted using the NucleoSpin RNA isolation kit from Macherey-Nagel (ref: 740955.240C). For patients and animal tissues a Trizol-based implementation of the NucleoSpin RNA isolation kit protocol was used as reported previously[59]. For all cases, 1 µg of total RNA was used for cDNA synthesis using qScript cDNA Supermix from Quanta (ref. 95048). Quantitative real-time PCR (rtPCR) was performed as previously described[51]. Universal Probe Library (Roche) primers and probes employed are detailed in Supplementary Table 8. β-ACTIN (Hs99999903_m1; Mm0607939_s1) and GAPDH (Hs02758991_g1, Mm99999915_g1) housekeeping assays from Applied Biosystems showed similar results (all quantitative rtPCR data presented were normalized using GAPDH/Gapdh).

Fatty acid oxidation was performed as previously described[51]. Lactate production was measured as referenced[60] using the Trinity Biotech lactate measurement kit.

Oxygen consumption rate (OCR) was measured with an XF24 extracellular flux analyser (Seahorse Bioscience)[61]. Briefly, 50,000 cells per well were seeded in an XF24 plate, and OCR measurements were normalized to cell number analysed by crystal violet. Cells were initially plated in 10% FBS DMEM media for 24 h, and 1 h before measurements, the medium was changed to serum- and bicarbonate-free DMEM, with glutamine and glucose (10 mM). Mitochondrial stress test was carried out using the following concentration of injected compound: oligomycin (1 µM).

For mitochondrial ATP assays, 50,000 PC3 and DU145 cells were plated onto 13-mm coverslips and transfected with a mitochondrial-targeted luciferase chimaera (mtLuc). Cells were perfused in the luminometer at 37 °C with KRB solution containing 25 µM luciferin and 1 mM CaCl₂ and supplemented with 5.5 mM glucose. Under these conditions, the light output of a coverslip of transfected cells was in the range of 5,000–20,000 c.p.s. for the luciferase construct versus a background lower than 100 c.p.s. Luminescence was entirely dependent on the presence of luciferin and was proportional to the perfused luciferin concentration between 20 and 200 µM.

Mitochondrial morphology was assessed by using a cDNA encoding mitochondrial matrix-targeted DsRed (mtDsRed). Cells were seeded onto 24-mm-diameter coverslips (thickness between 0.16–0.19 mm) (Thermo Scientific) and 24 h later cells were transfected with 2 µg mtDSred (Lipofectamine LTX reagent; Invitrogen). mtDsRed expression was assessed 36 h later. All of the acquisitions were performed with a confocal Nikon Eclipse T$_i$ system and fluorescent images were captured by using NisElements 3.2.

Lipid peroxidation based on MDA detection was assayed in xenograft samples following the manufacturer's instructions (MAK085 Sigma-Aldrich).

ROS production was determined by Mitosox and DCF staining as previously described[62].

Histopathological analysis. After euthanasia, histological evaluation of a haematoxylin and eosin (H&E)-stained section from formalin-fixed paraffin-embedded tissues of the following organs was performed: prostate gland, lymph nodes, long bones from lower limbs and other solid organs such as lungs and liver.

Following the consensus reported previously[63], prostate gland alterations were classified into four categories: gland within normal limits; high-grade prostatic intraepithelial neoplasia (HGPIN); HGPIN with focal micro-invasion; and invasive carcinoma. Lymphovascular invasion was assessed in all cases where micro-invasion foci or invasive carcinoma were observed.

Lymph node metastasis and the presence of groups of PCa cells in bone marrow were determined after haematoxylin–eosin (H&E) staining (lymph nodes) and immunohistochemical identification of cytokeratin (CK) and androgen receptor (AR)-expressing cells using a panCK rabbit polyclonal antibody (Dako) and AR rabbit polyclonal antibody (Santa Cruz Biotechnology, sc-816) (lymph nodes and bone marrow). In the case of bone marrow, cases were classified as 'dissemination negative' when none or few scattered (fewer than five) CK-expressing cells were identified and 'dissemination positive' when more than five or small groups of these cells were observed.

To assess the inflammatory component in the prostate tissues we performed a semiquantitative analysis in the glandular and the stromal areas separately for each of the specimens. We first determined the type of inflammatory cell present in each tissue compartment: polymorphonuclear neutrophils versus lympho-plasmacytic infiltrates. Then we performed a quantification of these cells using the following score system: 0—no inflammatory cells, 1—few cells, 2—moderate amount of cells and 3—high amount of cells. Scores in between were also determined as 0.5, 1.5 and 2.5. If both types of cell were present in one compartment, we chose the highest as the final score.

Proliferation was assessed in paraffin-embedded xenografts samples by using Ki67 antibody (MA5-14520, Thermo Scientific). Microvessel density was determined and quantified in GEMMs and xenograft samples by the immunodetection of CD31 (rabbit anti-CD31; Ref. ab28364 Abcam).

Metabolomics. Liquid-chromatography high-resolution mass spectrometry (LC–HRMS) metabolomics and stable isotope ^{13}C–U_6-glucose labelling was performed as reported previously[64–66]. Briefly, for LC–HRMS metabolomics, PC3 TRIPZ–HA–Flag–Pgc1a cells treated or untreated for 72 h with 0.5 µg ml^{-1} doxycycline were plated at 500,000 cells per well in 6-well plates, and grown maintaining the doxycycline regime for 42 h before collection. For stable isotope ^{13}C–U_6-glucose labelling experiments, 24 h after seeding cells were washed and exposed to media with serum, without glucose and pyruvate and supplemented 2 mM ^{13}C–U_6-glucose. After a further 16 h, cells were washed and another ^{13}C–U_6-glucose pulse was performed for 2 h before collection.

Transcriptomic analysis. For transcriptomic analysis in PC3 TRIPZ–HA–Flag–Pgc1α cells, the Illumina whole-genome -HumanHT-12_V4.0 (DirHyb, nt) method was used as reported previously[67].

Promoter enrichment analysis was assessed with the Transcription Factors (TFs) data set from MSigDB (The Molecular Signature Database; http://www.broadinstitute.org/gsea/msigdb/collections.jsp). The TFs data set contains genes that share a transcription factor-binding site defined in the TRANSFAC (version 7.4, http://www.gene-regulation.com) database. Each of these gene sets was annotated by a TRANSFAC record. A hypergeometric test was used to detect enriched data set categories.

The GSEA was performed using the GenePattern web tool from the Broad Institute (http://genepattern.broadinstitute.org). The list of PGC1α-upregulated genes ranked by their fold change was uploaded and analysed against a list of ERRα target genes[46]. The number of permutations carried out was 1,000 and the threshold was 0.05.

Bioinformatic analysis. For database normalization, all of the data sets used for the data mining analysis were downloaded from GEO, and subjected to background correction, $\log_2$ transformation and quartile normalization. In the case of using a pre-processed data set, this normalization was reviewed and corrected if required.

Frequency of alteration of metabolic co-regulators (Fig. 1 and Supplementary Fig. 1A): expression levels of the selected co-regulators were obtained from the data set reported by Taylor *et al.*[22]. A matrix containing signal values and clinical information was prepared to ascertain the up- or downregulation. We computed the relative expression of an individual gene and tumour to the expression distribution in a reference population (patients without prostate tumour or metastasis). The returned value indicates the number of standard deviations away from the mean of expression in the reference population (Z-score). Using a fold change of +2 and −2 as a threshold, we determined the number of samples from the cancer data set that were up- or downregulated. P values were calculated by comparing the means of normal of cancerous biopsies.

For quartile analysis in disease-free survival, patients' biopsies from primary tumours were organized into four quartiles according to the expression of the gene of interest in two data sets. The recurrence of the disease was selected as the event of interest. The Kaplan–Meier estimator was used to perform the test as it takes into account right-censoring, which occurs if a patient withdraws from a study. On the plot, small vertical tick marks indicate losses, where a patient's survival time has been right-censored. With this estimator we obtained a survival curve, a graphical representation of the occurrence of the event in the different groups, and a P value that estimates the statistical power of the differences observed.

For *PGC1A* genomic analysis, data from prostate cancer patients with copy number alteration information in Taylor[22], Grasso[21] and Robinson[25] *et al.* data sets were extracted from cbioportal.org. Percentage of shallow deletions of primary tumours and metastatic patients was calculated separately.

For correlation analysis, the Pearson correlation test was applied to analyse the relationship between paired genes. From this analysis, Pearson's coefficient (R) indicates the existing linear correlation (dependence) between two variables X and Y, giving a value between +1 and −1 (both included), where 1 is total positive correlation, 0 is no correlation, and −1 is total negative correlation. The P value indicates the significance of this R coefficient.
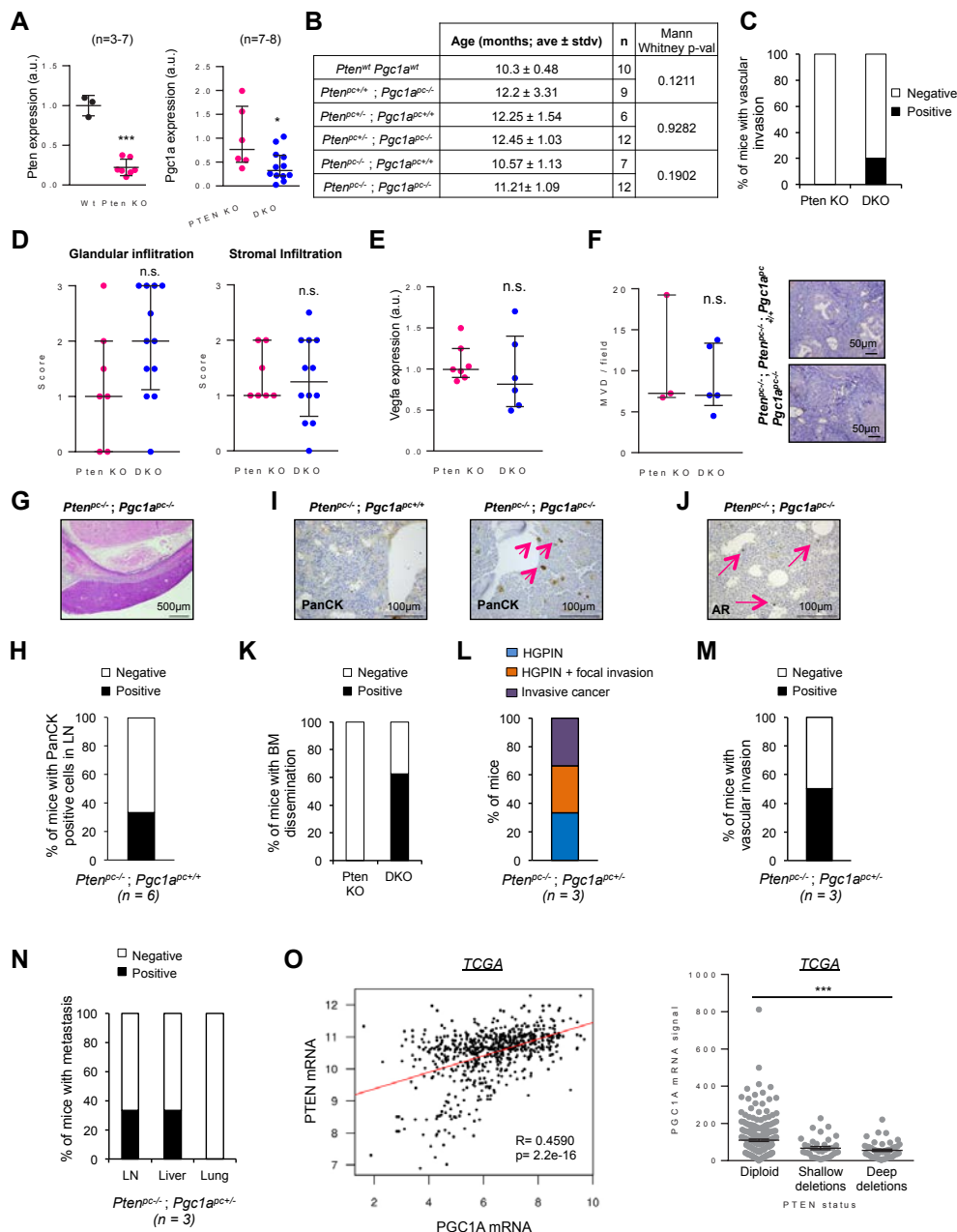
Statistics and reproducibility. No statistical method was used to predetermine sample size. The experiments were not randomized. The investigators were not blinded to allocation during experiments and outcome assessment. Unless otherwise stated, data analysed by parametric tests are represented by the mean ± s.e.m. of pooled experiments and median ± interquartile range for experiments analysed by non-parametric tests. n values represent the number of independent experiments performed, the number of individual mice or patient specimens. For each independent *in vitro* experiment, at least three technical replicates were used (exceptions: in western blot analysis technical replicates are presented, in untargeted metabolomics two technical replicates were used and for ^{13}C–U_6-glucose isotope labelling one technical replicate was used) and a minimum number of three experiments were performed to ensure adequate statistical power. For data mining analysis, ANOVA test was used for multi-component comparisons and Student's t-test for two component comparisons. In the *in vitro* experiments, normal distribution was confirmed or assumed (for $n < 5$) and Student's t-test was applied for two-component comparisons. For *in vivo* experiments, as well as for experimental analysis of human biopsies (from Basurto University Hospital) a non-parametric Mann–Whitney exact test was used, without using approximate algorithms to avoid different outcomes of statistics packages[68]. To this end, we applied the formulae described[69] for small-sized groups and Graphpad Prism for large-sized groups. In the statistical analyses involving fold changes, unequal variances were assumed. For contingency analysis, Fisher's exact test was used for two-group comparison (metastasis incidence) and Chi Square when analysing more than two groups (analysis of PGC1α–ERRα signature frequency in PCa human specimens). The confidence level used for all the statistical analyses was of 95% (alpha value = 0.05). Two-tailed statistical analysis was applied for experimental design without predicted result, and one-tail for validation or hypothesis-driven experiments.

Accession numbers and data sets. Primary accessions: the transcriptomic data generated in this publication have been deposited in NCBI's Gene Expression Omnibus and are accessible through GEO Series accession number GSE75193.

Referenced accessions: Grasso *et al.*[21], GEO: GSE35988; Lapointe *et al.*[18], GEO: GSE3933; Taylor *et al.*[22], GEO: GSE21032; Tomlins *et al.*[23], GEO: GSE6099; Varambally *et al.*[25], GEO: GSE3325.

53. Arroyo-Berdugo, Y. *et al.* Involvement of ANXA5 and ILKAP in susceptibility to malignant melanoma. *PLoS ONE* **9**, e95522 (2014).
54. Song, M. S. *et al.* Nuclear PTEN regulates the APC-CDH1 tumor-suppressive complex in a phosphatase-independent manner. *Cell* **144**, 187–199 (2011).
55. Chen, Z. *et al.* Differential p53-independent outcomes of p19(Arf) loss in oncogenesis. *Sci. Signal* **2**, ra44 (2009).
56. Nardella, C. *et al.* Differential requirement of mTOR in postmitotic tissues and tumorigenesis. *Sci. Signal* **2**, ra2 (2009).
57. Guiu, M., Arenas, E. J., Gawrzak, S., Pavlovic, M. & Gomis, R. R. Mammary cancer stem cells reinitiation assessment at the metastatic niche: the lung and bone. *Methods Mol. Biol.* **1293**, 221–229 (2015).
58. Carracedo, A. *et al.* Inhibition of mTORC1 leads to MAPK pathway activation through a PI3K-dependent feedback loop in human cancer. *J. Clin. Invest.* **118**, 3065–3074 (2008).
59. Ugalde-Olano, A. *et al.* Methodological aspects of the molecular and histological study of prostate cancer: focus on PTEN. *Methods* **77–78**, 25–30 (2015).
60. Finley, L. W. *et al.* SIRT3 opposes reprogramming of cancer cell metabolism through HIF1α destabilization. *Cancer Cell* **19**, 416–428 (2011).
61. Caro-Maldonado, A. *et al.* Metabolic reprogramming is required for antibody production that is suppressed in anergic but exaggerated in chronically BAFF-exposed B cells. *J. Immunol.* **192**, 3626–3636 (2014).
62. Wojtala, A. *et al.* Methods to monitor ROS production by fluorescence microscopy and fluorometry. *Methods Enzymol.* **542**, 243–262 (2014).
63. Ittmann, M. *et al.* Animal models of human prostate cancer: the consensus report of the New York meeting of the Mouse Models of Human Cancers Consortium Prostate Pathology Committee. *Cancer Res.* **73**, 2718–2736 (2013).
64. Liu, X. *et al.* High resolution metabolomics with acyl-CoA profiling reveals widespread remodeling in response to diet. *Mol. Cell. Proteomics* **14**, 1489–1500 (2015).
65. Liu, X., Ser, Z. & Locasale, J. W. Development and quantitative evaluation of a high-resolution metabolomics technology. *Anal. Chem.* **86**, 2175–2184 (2014).
66. Shestov, A. A. *et al.* Quantitative determinants of aerobic glycolysis identify flux through the enzyme GAPDH as a limiting step. *eLife* **3**, e03342 (2014).
67. Rodriguez, R. M. *et al.* Regulation of the transcriptional program by DNA methylation during human alphabeta T-cell development. *Nucleic Acids Res.* **43**, 760–774 (2015).
68. Bergmann, R., Ludbrook, J. & Spooren, W. P. J. M. Statistical computing and graphics: different outcomes of the Wilcoxon—Mann—Whitney test from different statistics packages. *Am. Statistician* **54**, 72–77 (2000).
69. Quinn, G. & Keough, M. *Experimental Design and Data Analysis for Biologists* (Cambridge Univ. Press, 2002).

Supplementary Figure 1 A, Expression of 23 metabolic co-regulators in Taylor[1] dataset (N: normal; PCa: prostate cancer). **B**, Expression of 7 metabolic co-regulators from figure 1a in four additional prostate cancer datasets (N: normal; PCa: prostate cancer). In Varambally[2] dataset gene expression levels are presented in Log$_2$. In Tomlins[3], Grasso[4] and Lapointe[5] datasets gene expression levels are presented in median centred Log$_2$. **C-D**, Association of *PGC1A* expression with Gleason score in TCGA provisional data[6,7] (C) and Taylor[1] datasets (D). **E**, Analysis of *PGC1A* expression in benign prostatic hyperplasia (BPH) and PCa specimens from Basurto University Hospital cohort (qRTPCR, BPH n= 14 patient specimens and Cancer n=16 patient specimens). **F**, *PGC1A* expression in normal prostate (N), primary tumour (PT) and metastatic (Met) specimens in *Grasso* dataset[4]. Points outlined by circles indicate statistical outliers (A, C, D and F). Error bars represent minimum and maximum values (A, B, C, D and F) or median with interquartile range (E). Statistic test: two-tailed Student T test (A, B), two-tailed Mann Whitney U test (E) and ANOVA (C, D and F).

A (n=3-7) (n=7-8)

Pten expression (a.u.) — Wt / Pten KO — ***

Pgc1a expression (a.u.) — PTEN KO / DKO — *

B

	Age (months; ave ± stdv)	n	Mann Whitney p-val
$Pten^{wt}\ Pgc1a^{wt}$	10.3 ± 0.48	10	0.1211
$Pten^{pc+/+}$; $Pgc1a^{pc-/-}$	12.2 ± 3.31	9	
$Pten^{pc+/-}$; $Pgc1a^{pc+/+}$	12.25 ± 1.54	6	0.9282
$Pten^{pc+/-}$; $Pgc1a^{pc-/-}$	12.45 ± 1.03	12	
$Pten^{pc-/-}$; $Pgc1a^{pc+/+}$	10.57 ± 1.13	7	0.1902
$Pten^{pc-/-}$; $Pgc1a^{pc-/-}$	11.21± 1.09	12	

C % of mice with vascular invasion — Pten KO / DKO — Negative / Positive

D Glandular infiltration / Stromal Infiltration — Score — Pten KO DKO — n.s.

E Vegfa expression (a.u.) — Pten KO DKO — n.s.

F MVD / field — Pten KO DKO — n.s. — $Pten^{pc-/-}$; $Pgc1a^{pc+/+}$ — $Pten^{pc-/-}$; $Pgc1a^{pc-/-}$ — 50µm

G $Pten^{pc-/-}$; $Pgc1a^{pc-/-}$ — 500µm

I $Pten^{pc-/-}$; $Pgc1a^{pc+/+}$ — PanCK 100µm — $Pten^{pc-/-}$; $Pgc1a^{pc-/-}$ — PanCK 100µm

J $Pten^{pc-/-}$; $Pgc1a^{pc-/-}$ — AR 100µm

H % of mice with PanCK positive cells in LN — $Pten^{pc-/-}$; $Pgc1a^{pc+/+}$ (n = 6) — Negative / Positive

K % of mice with BM dissemination — Pten KO / DKO — Negative / Positive

L % of mice — $Pten^{pc-/-}$; $Pgc1a^{pc+/-}$ (n = 3) — HGPIN / HGPIN + focal invasion / Invasive cancer

M % of mice with vascular invasion — $Pten^{pc-/-}$; $Pgc1a^{pc+/-}$ (n = 3) — Negative / Positive

N % of mice with metastasis — LN / Liver / Lung — $Pten^{pc-/-}$; $Pgc1a^{pc+/-}$ (n = 3) — Negative / Positive

O TCGA — PTEN mRNA vs PGC1A mRNA — R= 0.4590 p= 2.2e-16

TCGA — PGC1A mRNA signal — Diploid / Shallow deletions / Deep deletions — PTEN status — ***

Supplementary Figure 2 A, Analysis of *Pten* and *Pgc1a* gene expression in GEMMs of the indicated genotype (*Pten*wt *Pgc1a*wt n=3 mice; *Pten* pc-/- *Pgc1a*pc+/+ n=7 mice; *Pten*pc+/+ *Pgc1a*pc-/- n=6 mice; *Pten*pc-/- *Pgc1a*pc-/- n=12 mice; data is normalized to *Gapdh* expression). **B**, Age comparison between experimental cohorts (n as in Figure 2d). **C**, Quantification of prostate tissue with histological vascular invasion signs in *Pten* KO (2 mice) and DKO mice (9 mice) (limited to mice with invasive signs). **D**, Histological analysis of inflammatory signs (stromal and glandular infiltration) in *Pten* KO and DKO mice (*Pten* KO, n=7 mice; DKO, n=12 mice). **E** Quantification of *Vefga* mRNA expression in *Pten* KO and DKO mice (*Pten* KO, n=7 mice; DKO, n=6 mice; data is normalized to *Gapdh* expression). **F**, Quantification of microvessel density (MVD) (dot plot, left panels) and representative images of CD31 immunodetection (right panels) in *Pten* KO and DKO mice (*Pten* KO, n=3 mice; DKO, n=5 mice). **G**, Representative haematoxylin and eosin staining depicting liver metastasis in DKO (bar=500µm). **H**, Incidence of small groups of Pan-cytokeratin (Pan-CK) positive cells in the lymph nodes of *Pten* KO mice (6 mice). **I-J**, representative immunohistochemical detection (200X) of Pan-CK positive

cells in the bone marrow (BM) of *Pten* KO and DKO (I) and androgen receptor (AR) in the bone marrow of DKO (J) (bar=100µm). Pink arrows indicate immunoreactive cells. **K**, Quantification of BM dissemination frequency (*Pten* KO, 6 mice; DKO, 8 mice). **L-M**, Histopathological characterization of the prostate tissue (L) and frequency of vascular invasion signs (M, only in mice with invasion signs) in *Pten*pc-/-, *Pgc1a*pc+/- mice (3 mice). **N**, Frequency of metastatic lesions in lymph nodes (LN), liver and lung of *Pten*pc-/-, *Pgc1a*pc+/- mice (3 mice). **O**, Correlation between *PGC1A* and *PTEN* gene expression in prostate cancer specimens (left panel) and the association of *PTEN* genomic loss to *PGC1A* gene expression (right panel), in TCGA provisional dataset. pc, prostate-specific allelic changes; +, Wildtype allele; -, deleted allele; wt: any given genotype resulting in the lack of deletion of *Pgc1a* and *Pten* alleles. *Pten* KO = *Pten*pc-/-, *Pgc1a*pc+/+; DKO = *Pten*pc-/-, *Pgc1a*pc-/-. Stdv: standard deviation of the mean. All error bars represent median with interquartile range. p = p-value. a.u: arbitrary units. Statistic tests: one-tailed Mann-Whitney U test (A, B), two-tailed Mann-Whitney U test (D, E and F); ANOVA (O, right panel); Pearson´s coefficient (O, left panel). *p < 0.05, ***p < 0.001.
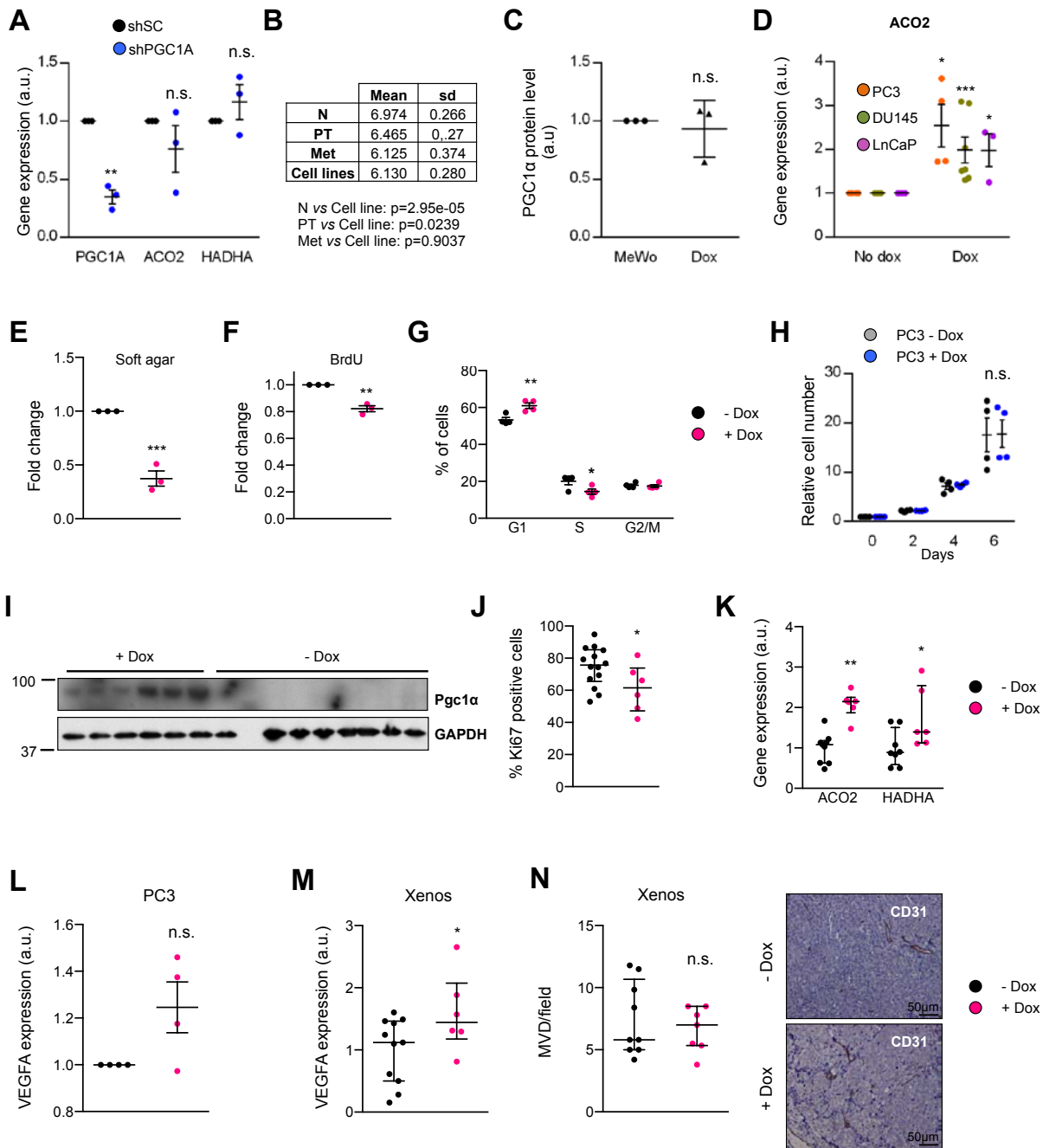
Supplementary Figure 3 A, mRNA expression of *PGC1A*, *ACO2* and *HADHA* by qRTPCR in PC3 cells transduced with scramble shRNA (shSC) or *PGC1A*-targeting shRNA (shPGC1A) (n=3). **B**, *PGC1A* expression in normal (N, n=29), primary tumour (PT, n=131), metastasis (Met, n=19) specimens and metastatic cell lines. Data is shown as Log$_2$ mRNA expression. **C**, Densitometry of PGC1α protein expression in MeWo (endogenous) and PC3 TRIPZ-HA-Pgc1α (ectopic) cell lines, relative to β-Actin (n=3, independent experiments). **D**, Effect of Pgc1α induction (+Dox) on *ACO2* mRNA expression in PC3 (n=4, independent experiments), DU145 (n=7, independent experiments) and LnCaP cells (n=3, independent experiments). **E-F**, Effect of Pgc1α expression on anchorage-independent growth (E, n=3, independent experiments) and BrdU incorporation (F, n=3, independent experiments) in DU145 cells. **G**, Effect of Pgc1α expression on cell cycle progression in PC3 cells (n=4, independent experiments). **H**, Effect of

doxycycline treatment (0.5µg/ml) on cell growth of non-transduced PC3 cells (n=3, independent experiments). **I-J**, Pgc1α protein expression and cell proliferation by Ki67 immunoreactivity in xenograft samples from Fig. 3f (- Dox n=14 tumours, + Dox n=6 tumours). **K**, mRNA expression of ACO2 and HADHA in xenograft samples from Fig. 3f. (- Dox n=9 tumours, + Dox n=6 tumours). **L-M**, Analysis of VEFGA mRNA expression upon Pgc1α induction in PC3 cells (L, n=4, independent experiments) and xenograft samples (M, - Dox n=9 tumours and + Dox n=6 tumours). **N**, Quantification of microvessel density (MVD) in xenograft samples (- Dox n=9 tumours and + Dox n=7 tumours). Right panels show representative CD31 staining micrographs. Error bars indicate s.e.m (A, C, D, E, F, G, H, L) and median with interquartile range (J, K, M, N). Statistic tests: two-tailed Student T test (A, B, C, D, E, F, G, H, L) and one-tailed Mann-Whitney U test (J, K, M, N). *p < 0.05, **p < 0.01, ***p < 0.001.
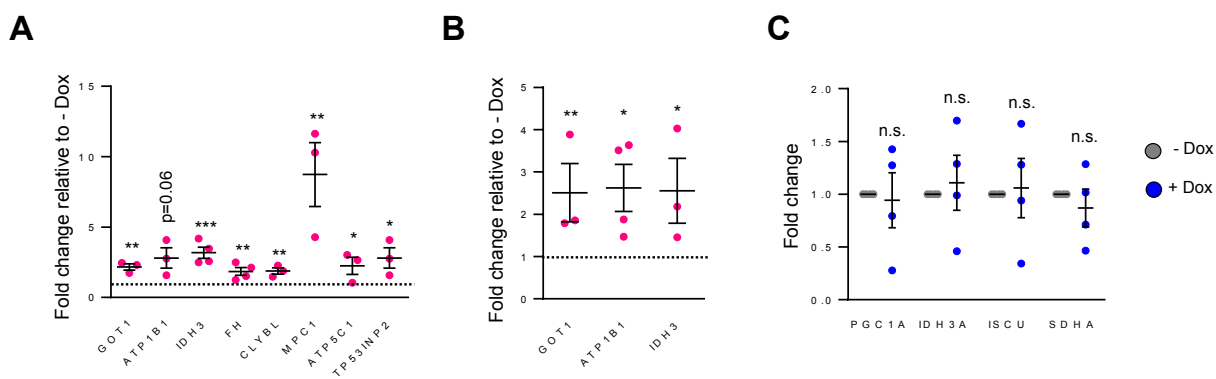
Supplementary Figure 4 A-B, Validation of the microarray by qRTPCR in DU145 (n=4, independent experiments) and LnCaP (n=3, independent experiments) TRIPZ-HA-Pgc1a cells. Gene expression values relative to - Dox cells are represented (reference - Dox gene expression values are indicated with a dotted line) **C**, mRNA expression of PGC1α target genes in doxycycline-treated (0.5μg/ml) non-transduced PC3 cells (n=3, independent experiments). Error bars represent s.e.m. Statistic test: One tail Student T test. *p < 0.05, **p < 0.01, ***p < 0.001.
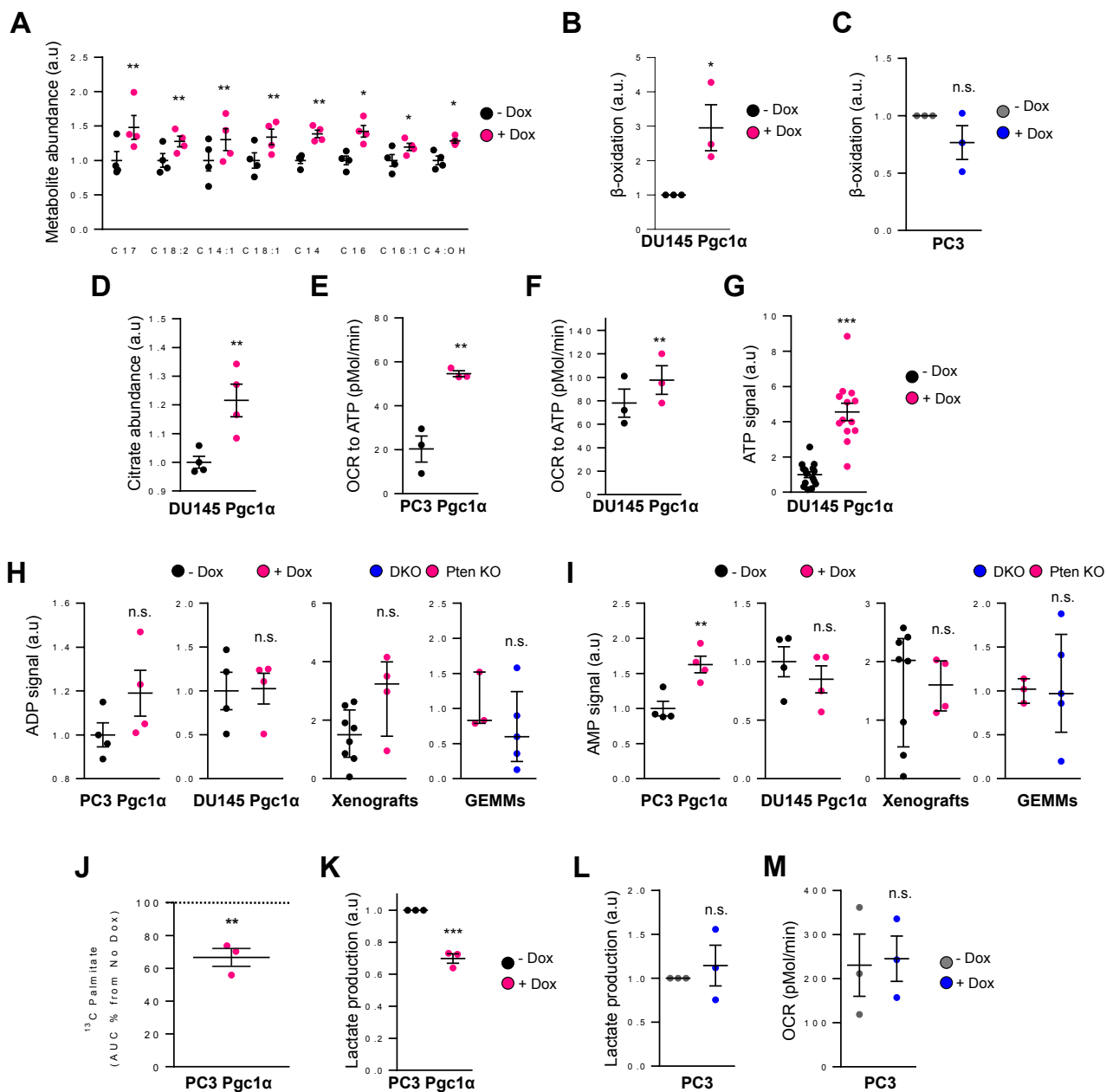
Supplementary Figure 5 A, Analysis of differential abundance in metabolites involved in fatty acid catabolism by untargeted LC-HRMS in DU145 TRIPZ-HA-Pgc1α cells (n=4, independent experiments). **B-C** Evaluation of the dehydrogenation of ^{3}H-palmitate (readout of β-oxidation) in DU145 cells upon Pgc1α expression (B, n=3, independent experiments) and, in doxycycline-treated (0.5μg/ml) non-transduced PC3 cells (C, n=3, independent experiments). Values relative to - Dox cells are presented. **D**, Effect of Pgc1α expression on citrate abundance measured by LC-HRMS metabolomics in DU145 cells (n=4, independent experiments). **E-F**, ATP-producing OCR (upon complex V inhibition by oligomycin injection) in PC3 (E, n=3, independent experiments) and DU145 (F, n=3, independent experiments) cells upon Pgc1α expression. **G**, Basal mitochondrial ATP production in DU145 cells upon Pgc1α expression (n=10, independent experiments). **H-I**, LC-HRMS quantification of ADP (H) and AMP (I)

abundance in PC3 Pgc1α (n=4, independent experiments), DU145 Pgc1α (n=4, independent experiments), xenografts (- Dox n=8 tumours; + Dox n=4 tumours) and GEMMs (*Pten* KO n=3 mice; DKO n=5 mice). **J**, Quantification of area under the curve (AUC, relative to - Dox) of Palmitate labelling from ^{13}C-U$_6$-Glucose in PC3 TRIPZ-HA-Pgc1α cells (data related to Fig. 5j, n=3, independent experiments). **K**, Determination of extracellular lactate in PC3 TRIPZ-HA-Pgc1α cells (n=3, independent experiments). **L-M**, Lactate production (L) and OCR (M) in doxycycline-treated (0.5μg/ml) non-transduced PC3 cells (n=3, independent experiments). Error bars represent s.e.m., except xenograft and GEMM data in H-I, that represent median with interquartile range. Statistic tests: two tailed Student T test (A, B, C, D, E, F, G, H (PC3 and DU145), I (PC3 and DU145), J, K, L, M) and one tailed Mann Whitney U test (H (Xenografts and GEMMs), I (Xenografts and GEMMs)). *p < 0.05, **p < 0.01, ***p < 0.001.
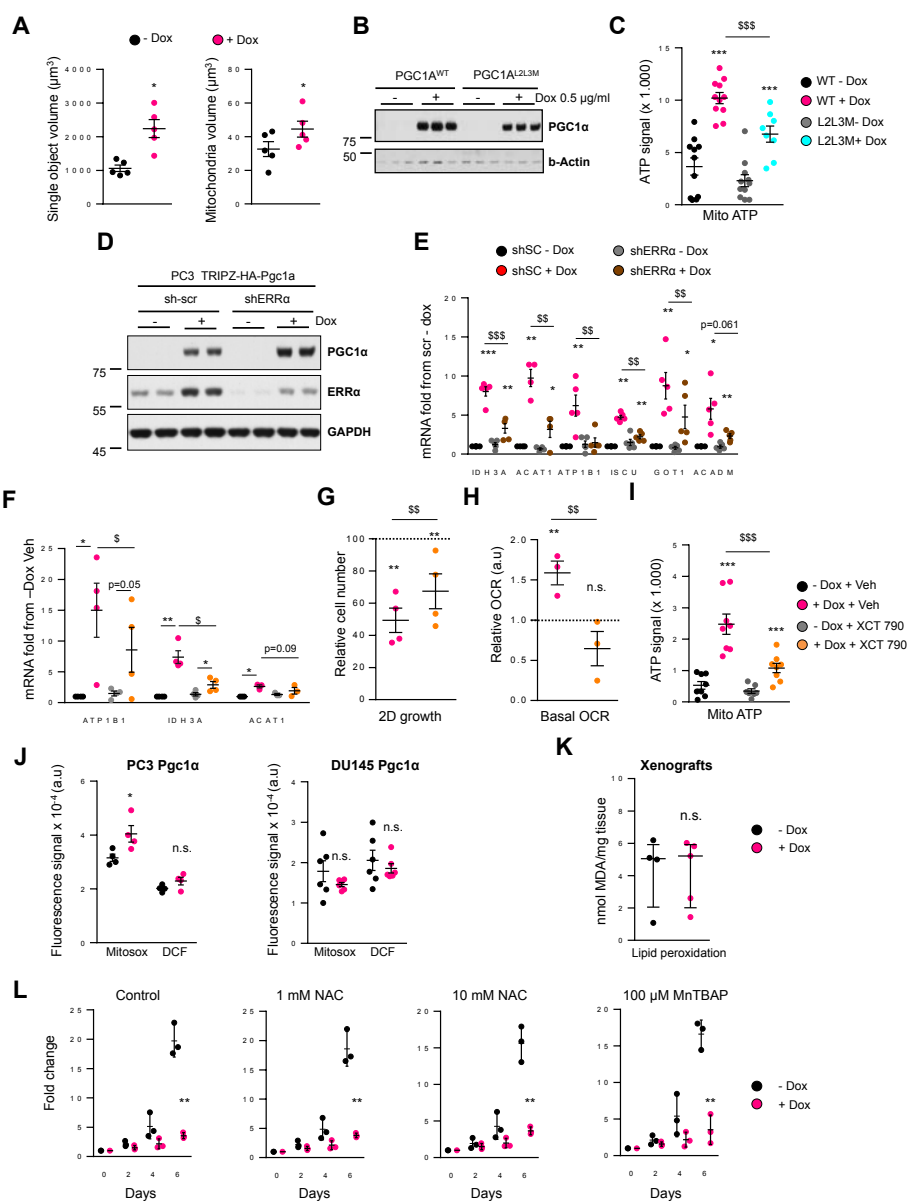
Supplementary Figure 6 A, Analysis of mitochondrial morphology (mitochondrial volume) in PC3 cells upon Pgc1α expression (n=5, independent experiments). B, Expression of PGC1αWT and PGC1αL2L3M in PC3 cells after treatment with 0.5 µg/ml doxycycline (Dox) (a representative experiment with technical replicates is presented, similar results were obtained in three independent experiments). C, Basal mitochondrial ATP production in PGC1αWT and PGC1αL2L3M PC3 cells (n=11, independent experiments). D, Expression of Pgc1α and ERRα in doxycycline-treated PC3 TRIPZ-HA-Pgc1α cells transduced with sh-scramble (shSC) or shERRα (a representative experiment with technical replicates is presented, similar results were obtained in three independent experiments). E, mRNA expression of PGC1α target genes in doxycycline-treated PC3 TRIPZ-HA-Pgc1α cells transduced with shSC or shERRα (n=4 for ACAT1 and n=5 for IDH3A, ATP1B1, ISCU, GOT1 and ACADM; independent experiments). F-I, mRNA expression of PGC1α target genes (F, n=3 for ACAT1 and n=4 for ATP1B1 and IDH3A; independent experiments), cell number (G, n=4, independent experiments), basal oxygen consumption (H, n=3, independent experiments) and basal mitochondrial ATP production

(I, n= 7 for - Dox + XCT790; n=8 the rest; independent experiments) in vehicle (Veh) or XCT790-treated Pgc1α-inducible PC3 cells. J, Evaluation of cellular (DCF) and mitochondrial-specific (Mitosox) ROS production in Pgc1α-expressing PC3 (left panel; n=4, independent experiments) and DU145 (right panel; n=6, independent experiments) cells. K, Evaluation of lipid peroxidation in xenograft tissues from Fig. 3f (- Dox n=4 tumours; + Dox n=5 tumours). L, Effect of the indicated antioxidant treatments on cell number (relative to day 0) of Pgc1α-expressing PC3 cells (n=3, independent experiments). DCF: 2',7'-dichlorodihydrofluorescein. n.s.: not significant. Error bars represent s.e.m. (A, C, E, F, G, H, I, J, L) or median with interquartile range (K). Statistic tests: two tailed Student T test (A, C, E, F, G, H, I, J, L) or one tailed Student T test (comparison between + Dox conditions in C, E, F, G, H, I) and two tailed Mann-Whitney U test (K). */$ p < 0.05, **/$$ p < 0.01, ***/$$$ p < 0.001. Asterisks indicate statistic between - Dox and + Dox conditions (unless represented otherwise) and dollar symbol between either, vehicle (Veh) and XCT790-treated Pgc1α-expressing cells, shSC and shERRa-transduced Pgc1α-expressing cells or Pgc1αWT and Pgc1αL2L3M.
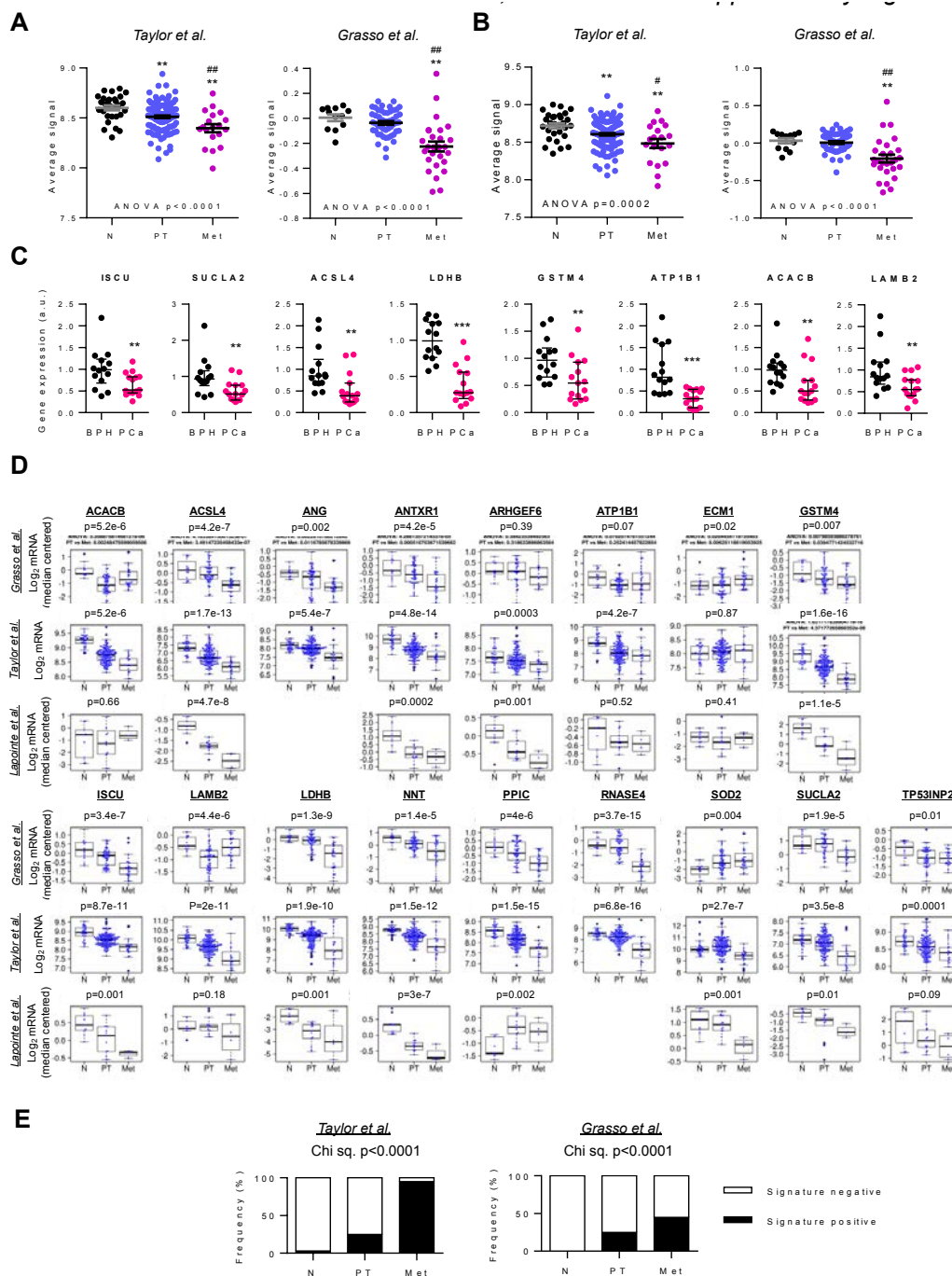
Supplementary Figure 7 A-B, Representation of the average signal of genes within the PGC1α-upregulated gene set (A) (Fig. 7b, blue circle) and within the PGC1α-dependent ERRα-upregulated gene set (B) (Fig. 7b, yellow circle, Table S6) in the indicated datasets[1,4,6,7], in normal (N; Taylor n=29 and Grasso n=12), primary tumours (PT; Taylor n=131 and Grasso n=49) and metastasis (Mets; Taylor n=19 and Grasso n=27). **C**, qRTPCR mRNA expression analysis of PGC1α target genes from C, in benign prostatic hyperplasia (BPH) and PCa specimens from Basurto University Hospital cohort (BPH n=14 patient specimens; Prostate cancer n=16 patient specimens). **D**, Expression of the indicated genes (from Supplementary Table 7) in different disease states (N: normal, Lapointe n=9, Taylor n=29 and

Grasso n=12; PT: primary tumour, Lapointe n= 13, Taylor n=131 and Grasso n=49; Met: metastasis, Lapointe n=4, Taylor n=19 and Grasso n=27) in three PCa datasets[1,4,5]. **E**, Representation of "PGC1α-ERRα Q1 signature" frequency within different tumour types (N: normal; PT: primary tumour; Met: metastasis) in two datasets[1,4] (Taylor: N, n=29; PT, n= 131; Met, n=19; Grasso: N, n=12; PT, n=49; Met, n=27). Error bars represent s.e.m. (A, B), median with interquartile range (C) and maximum and minimum (D). Statistic tests: Statistic tests: ANOVA (A, B, D); two tailed Student T test (A, B), one tailed Mann Whitney U test (C), Chi Square (E). Asterisks in A, B indicates statistics between normal and metastasis and hash between primary tumours and metastasis. p: p-value. */# p < 0.05, **/## p < 0.01, ***p < 0.001.

A

M: Marker (Precision Plus Protein™ Dual Color Standards, Ref #1610374)

B

C

D

E
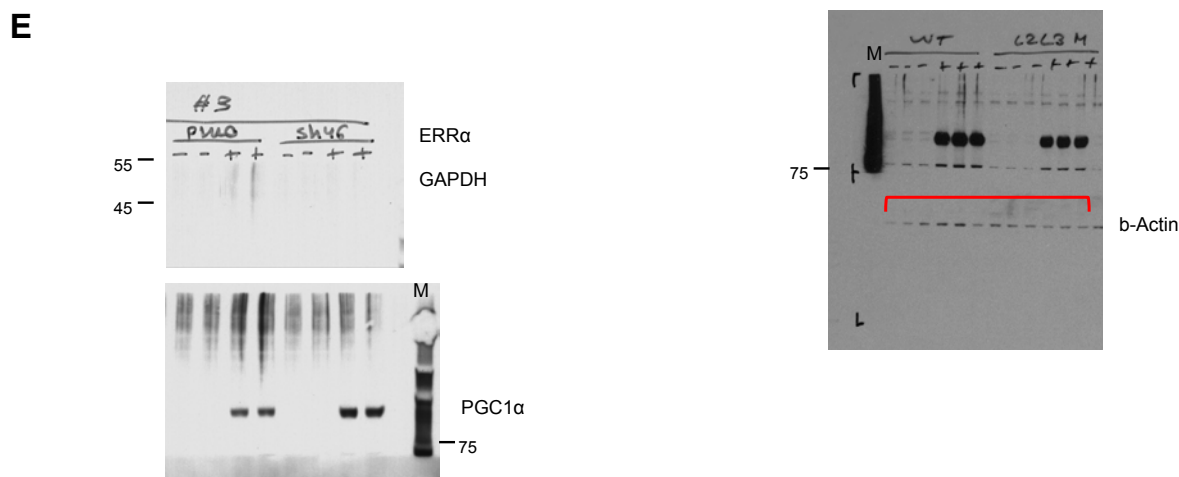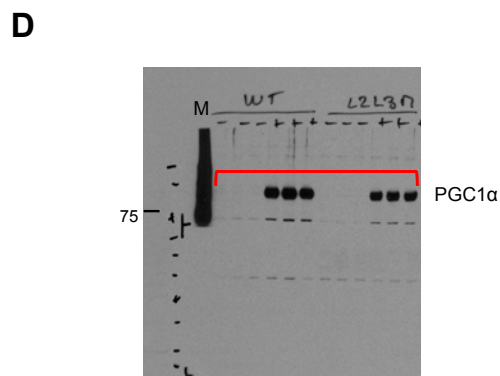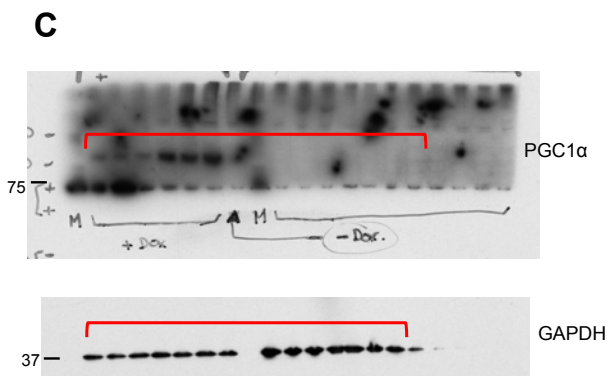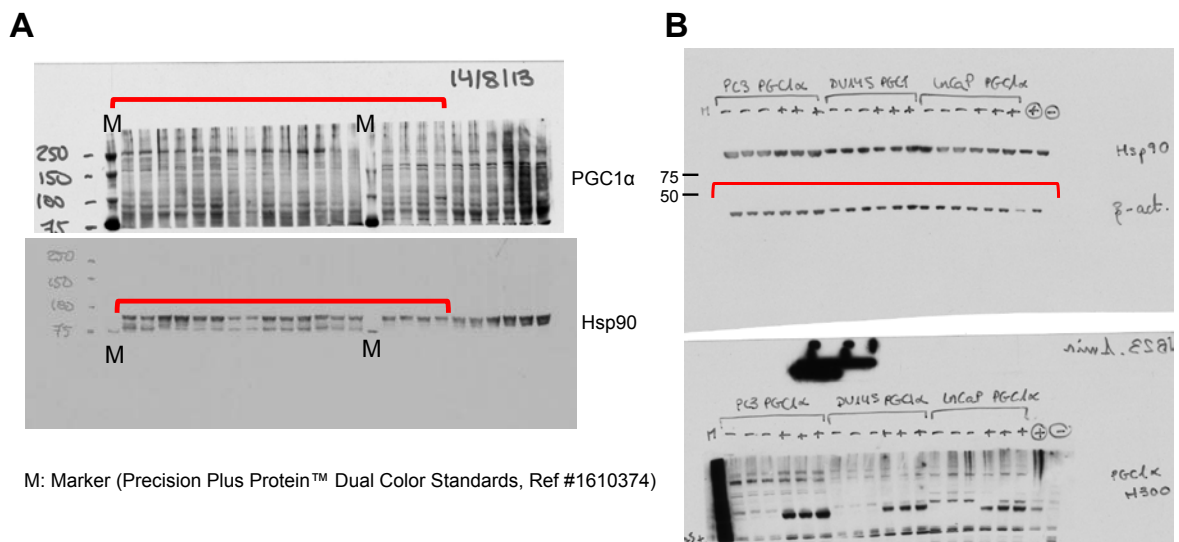
M: Marker (Pink Prestained protein ladder, Nippon Genetics, Cat.No. MWP02)

Supplementary Figure 8 Unprocessed blots. **A**, Western blot corresponding to Figure 3a. **B**, Western blot corresponding to Figure 3b. **C**, Western blot corresponding to Supplementary Figure 3I. **D**, Western blot corresponding to Supplementary Figure 6B. **E**, Western blot corresponding to Supplementary Figure 6D. Precision Plus Protein™ Dual Color Standards (Ref #1610374) markers was used in A-D. Pink Pre-stained protein ladder, Nippon Genetics, Cat.No. MWP02, was used in E.

Table titles and legends

Supplementary Table 1 Gene expression profiling in PC3 TRIPZ-HA-Pgc1α cells (Doxycycline vs. No Doxycycline, (0.5μg/ml).

Supplementary Table 2 Untargeted LC-HRMS metabolomic profiling in PC3 TRIPZ-HA-Pgc1α cells (Doxycycline vs. No Doxycycline, (0.5μg/ml).

Supplementary Table 3 Untargeted LC-HRMS metabolomic profiling in DU145 TRIPZ-HA-Pgc1α cells (Doxycycline vs. No Doxycycline, (0.5μg/ml).

Supplementary Table 4 Untargeted LC-HRMS metabolomic profiling in xenograft-derived tissues (from PC3 TRIPZ-HA-Pgc1α cells) upon induction of Pgc1α expression (Doxycycline diet vs. chow).

Supplementary Table 5 Untargeted LC-HRMS metabolomic profiling in GEMM-derived prostate tissues ($Pten^{pc-/-}$, $Pgc1a^{pc-/-}$ vs. $Pten^{pc-/-}$, $Pgc1a^{pc+/+}$).

Supplementary Table 6 Definition of ERRα signature within the PGC1α gene list. Genes included in the TGACCTY_V$ERR1_Q2 dataset or identified in the study by Stein et al (STEIN_ESRRA_TARGETS[8]) were considered as ERRα targets.

Supplementary Table 7 List of Pgc1α-regulated genes in PC3 (Supplementary Table 1) that show significant and consistent correlation with *PGC1A* in human prostate cancer datasets (R>0.2; p<0.05) in at least three out five datasets.

Supplementary Table 8 List of primers and probes (Universal Probe Library, Roche) used in qRTPCR.

Supplementary Table 9 Statistics source data for animal experiments reported in Fig. 3k, and Fig. 6e, h. All data are organized into different sheets and named based on the corresponding figure/panel numbers.

References:

1   Taylor, B. S. *et al.* Integrative genomic profiling of human prostate cancer. *Cancer Cell* **18**, 11-22, doi:10.1016/j.ccr.2010.05.026 (2010).

2   Varambally, S. *et al.* Integrative genomic and proteomic analysis of prostate cancer reveals signatures of metastatic progression. *Cancer Cell* **8**, 393-406, doi:10.1016/j.ccr.2005.10.001 (2005).

3   Tomlins, S. A. *et al.* Integrative molecular concept modeling of prostate cancer progression. *Nat Genet* **39**, 41-51, doi:10.1038/ng1935 (2007).

4   Grasso, C. S. *et al.* The mutational landscape of lethal castration-resistant prostate cancer. *Nature* **487**, 239-243, doi:10.1038/nature11125 (2012).

5   Lapointe, J. *et al.* Gene expression profiling identifies clinically relevant subtypes of prostate cancer. *Proc Natl Acad Sci U S A* **101**, 811-816, doi:10.1073/pnas.0304146101 (2004).

6   Cerami, E. *et al.* The cBio cancer genomics portal: an open platform for exploring multidimensional cancer genomics data. *Cancer Discov* **2**, 401-404, doi:10.1158/2159-8290.CD-12-0095 (2012).

7   Gao, J. *et al.* Integrative analysis of complex cancer genomics and clinical profiles using the cBioPortal. *Sci Signal* **6**, pl1, doi:10.1126/scisignal.2004088 (2013).

8   Stein, R. A. *et al.* Estrogen-related receptor alpha is critical for the growth of estrogen receptor-negative breast cancer. *Cancer Res* **68**, 8805-8812, doi:10.1158/0008-5472.CAN-08-1594 (2008).